(Preprint) AAS 26-113

GENERALIZED BACKSUBSTITUTION DYNAMICS FOR BRANCHING OF FREE RIGID BODIES ATTACHED TO PRESCRIBED COMPONENTS

Leah Kiner* **and Hanspeter Schaub†**

While often tedious and time-consuming, deriving the equations of motion for spacecraft systems is essential in order to simulate spacecraft missions and ensure performance requirements are met. A complete analytic rederivation, software implementation, and verification of the equations is typically required if any changes are made to the original spacecraft configuration. To avoid this unfavorable process, this work introduces a new, generalized backsubstitution formulation for branching of spacecraft components using a joint mapping representation. Development of this formulation enables a spacecraft system to be easily simulated and reconfigured throughout the entire mission design process, without requiring any analytic rederivations, software modifications, or verification when the spacecraft design is modified. Building on previous work, which expanded the backsubstitution method to enable branching of specific dynamic components relative to prescribed motion components, this work develops a generalized formulation for attachment of free six degree-of-freedom rigid bodies to prescribed motion components. This new development enables a wide variety of previously impossible spacecraft configurations to be simulated using the backsubstitution method.

INTRODUCTION

Spacecraft missions have seen rapid advancements over the last several decades. The 1957 launch of the first artificial satellite, Sputnik 1— a small sphere with simple sensors— marked the inception of the space age. Within the next year, spacecraft progressed to contain strut-mounted solar "paddles" first seen on Pioneer 5, which later advanced to deployable fixed-orientation solar panels beginning in 1961 with the Ranger series and the Lunar Orbiter 1 in 1966. By 1973, the US launched Mariner 10, the first two-wing gimbaled solar array design that enabled tracking of the Sun. This concept, together with the cheaper hub-fixed panel design, remain in primary use today.[1]

The latest missions to the farthest edges of our solar system have required critical component advancements in order to navigate through deep space efficiently. The Lucy mission to the Trojan asteroids, the Emirates Mission to the Asteroid Belt (EMA), and the Double Asteroid Redirection Test (DART) binary asteroid impact mission all required extensive solar array advancements to meet power requirements. The Lucy and EMA missions use two large circular flexible-substrate solar arrays which deploy using a motor-driven lanyard and articulate to track the Sun.[2–5] Similarly, the DART mission was the first of its kind to demonstrate roll-out solar array (ROSA) technology.[2,6,7]

*Graduate Research Assistant, Ann and H.J. Smead Department of Aerospace Engineering Sciences, University of Colorado Boulder, Colorado Center For Astrodynamics Research, Boulder, CO, 80303 USA. leah.kiner@colorado.edu

†Professor and Department Chair, Schaden Leadership Chair, Ann and H.J. Smead Department of Aerospace Engineering Sciences, University of Colorado, Boulder, 431 UCB, Colorado Center for Astrodynamics Research, Boulder, CO, 80309. AAS Fellow, AIAA Fellow.

To meet thrust vector alignment requirements for deep-space missions such as EMA, Deep Space 1,[8] Dawn,[9] and Psyche,[10] spacecraft ionic thrusters evolved from being hub-fixed to being mounted on gimbaled platforms.[5,11–13]

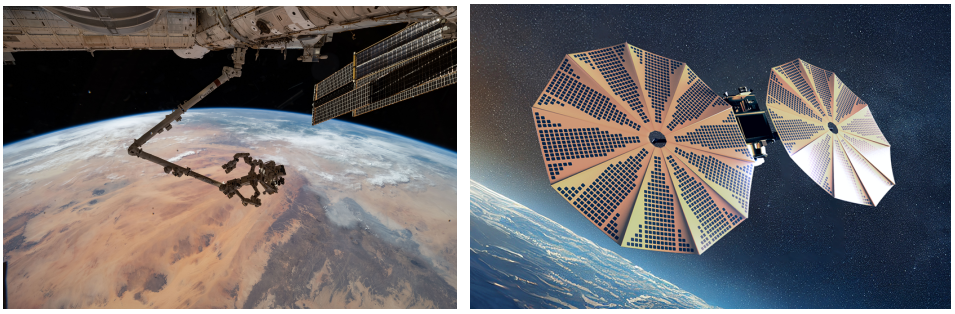

(a) Canadarm2[14] (b) EMA MBR Explorer[15]

Figure 1. Examples of complex multi-body spacecraft missions.

The desire to send humans into space for extended periods drove advancements required for space orbiters including the Space Shuttle orbiter and the International Space Station, where multi-link robotic arms such as the space station remote manipulator system (Canadarm),[16,17] were developed to aid in complex orbital servicing, assembly, and docking operations. The football-field-sized International Space Station particularly illustrates the evolution of spacecraft complexity, containing a massive articulated main truss to which other large components—such as the Canadarm, solar panels, and experimental modules—are attached.[18] The Lunar Gateway is proposed to utilize a third generation of the Canadarm for similar tasks. Modeling and simulation of these complex spacecraft systems is a fundamental part of spacecraft mission design, providing a necessary method of analyzing and validating expected mission performance.

The field of multi-body dynamics and its applications to spacecraft systems has been studied for many decades.[18–29] There are many different methods for deriving the equations of motion (EOM) for multi-body systems, some of which include Newtonian and Eulerian mechanics, Lagrangian mechanics, and Kane's method.[30,31] Although developing the EOM for complex rigid body systems is not a nontrivial task, perhaps the most difficult and important consideration in multi-body dynamics is how the EOM are formulated and implemented in software. This choice dramatically influences the long-term maintainability, scalability, testability, and computational efficiency of the software. Research efforts have focused deeply on this aspect of multi-body dynamics.

To solve the inverse dynamics problem of computing the joint forces required to produce given active joint velocities and accelerations, Luh et al. coined the $\mathcal{O}(n)$ recursive Newton-Euler method.[24] Walker and Orin first introduced the $\mathcal{O}(n^2)$ composite-rigid-body algorithm (CRBA) to compute the mass matrix for a kinematic tree, which was later improved and modified to be more efficient.[25,32] Featherstone later introduced a six-dimensional vector notation called spatial notation, where the linear and angular components of the rigid body motion are combined to yield a unified set of equations.[32–34] This approach greatly reduces the size and number of equations required to facilitate dynamics analysis and has been shown to significantly improve computational efficiency through recursive relations.[35] Improving the $\mathcal{O}(n^2)$ CRBA, Featherstone developed the $\mathcal{O}(n)$ forward dynamics articulated-body algorithm (ABA) which has been used in many robotics applications.[34] Spatial Operator Algebra (SOA) is a similar, widely applied dynamics formulation capable of sim-

ulating flexible multi-body systems efficiently in software using a reformulated spatial vector notation.[36–38] Used in the Jet Propulsion Laboratory's Dynamics Algorithms for Real-Time Simulation (DARTS) [*] software package, the method leverages linear operators acting on spatial vectors to derive more general recursive solutions. NASA's open-source software package 42 [†] utilizes a tree-topology approach for implementation of the spacecraft dynamics, which reduces the size of the system mass matrix for numerical integration.[19,21]

The backsubstitution method (BSM) is a spacecraft dynamics formulation that has been recently developed to prioritize the issues of computational efficiency, modularity, scalability, and testability of spacecraft-specific simulation software.[39–42] The original foundation of this method is the assumption of hub-centric spacecraft configurations, where all of the system components (effectors) such as solar panels, reaction wheels, and thrusters are attached to a central rigid hub structure. While this assumption limits the spacecraft design space, it encompasses a sufficiently wide spectrum of allowable spacecraft configurations and has proven to adequately support near-Earth and interplanetary space missions. Moreover, this requirement provides several advantages from a software perspective. The first is that the dynamics of each component are decoupled from one another in the system mass matrix. This observation enables all component accelerations to be analytically back-substituted into the hub dynamics and decouples the hub EOM from the other system components. This analytic process achieves a significant numerical simulation speed increase and reduces the computational load for large multi-body spacecraft systems because the entire system mass matrix no longer needs to be inverted. Instead, only two 3×3 matrix inversions are required to solve for the hub accelerations.[39,41] The second advantage of this method is its modular nature with which it can be implemented in software, which is strongly tied to its other testability and scalability advantages. Because all component dynamics are decoupled from one another, the EOM for each type of component attachment to the hub need only be derived and implemented modularly in software once, allowing for both scalability of the spacecraft system and a straightforward, independent verification process for each dynamics model. The benefits of this dynamics formulation cannot be overstated. Especially for spacecraft mission design and analysis, rederivation of the system EOM is nearly always required and can be an extremely time-intensive process even for simple changes to the spacecraft design. This method enables rapid reconfiguration of the spacecraft design without requiring rederivation of the system EOM.[39]

Prior work using the backsubstitution method has developed the EOM for a wide variety of components attached to a spacecraft hub including single and multi-hinged solar panels,[43] reaction wheels,[44] control moment gyroscopes,[45] linear fuel slosh particles,[46] and spherical pendulum slosh particles.[47] Recent work by Carneiro et al. developed more general formulations to simulate chains of sequentially rotating or translating rigid bodies.[48–50] The results can be used to simulate telescoping or rotatable robotic arms and other chained structures. Kiner et al. recently expanded the backsubstitution method to simulate prescribed spacecraft components, enabling branching in the spacecraft configuration space that was not feasible before.[51] Most recently, Kiner et al. introduced a method to simulate branching not limited to prescribed spacecraft components, but instead permits branching of specific one and two-axis rotating rigid bodies relative to prescribed components.[52] These new developments *modified* existing backsubstitution formulations for attachment to prescribed motion components, rather than introducing new branching components in software. This paper directly builds upon this previous branching work by introducing a generalized single-

[*] `https://dartslab.jpl.nasa.gov/DARTS/index.php`
[†] `https://software.nasa.gov/software/GSC-16720-1`

body branching formulation using a joint mapping representation. The results can be used to simulate six degree-of-freedom rigid component motion relative to prescribed motion components.

The organization of this paper is as follows: First, an overview of the spacecraft dynamics backsubstitution method is provided. Next, the problem statement for the general branching system and the joint mapping formulation and kinematics are outlined. The general equations of motion for the single-body branching system are next derived, including the system's translational and rotational equations of motion and the general rigid body equations of motion. Finally, the equations are organized into the backsubstitution formulation and an example scenario illustrating the applicability of the branching formulation is provided. The concluding remarks are offered in the final section of this paper.

BACKSUBSTITUTION METHOD REVIEW

This paper expands the allowable configuration space for complex multibody spacecraft systems under the assumptions of the backsubstitution method. As discussed previously, the formulation was originally developed using a hub-centric design assumption to address the issues of software modularity, scalability, maintainability, and testability.[39–41] The formulation enables complex multi-body spacecraft simulations to be rapidly configured, executed, and tested in software. The hub-centric design requirement produces the following general form for the system mass matrix

$$\begin{bmatrix} [\cdot]_{3\times3} & [\cdot]_{3\times3} & [\cdot]_{3\times1} & [\cdot]_{3\times1} & \cdots & [\cdot]_{3\times1} \\ [\cdot]_{3\times3} & [\cdot]_{3\times3} & [\cdot]_{3\times1} & [\cdot]_{3\times1} & \cdots & [\cdot]_{3\times1} \\ [\cdot]_{1\times3} & [\cdot]_{1\times3} & [\cdot]_{1\times1} & [0]_{1\times1} & \cdots & [0]_{1\times1} \\ [\cdot]_{1\times3} & [\cdot]_{1\times3} & [0]_{1\times1} & [\cdot]_{1\times1} & \cdots & [0]_{1\times1} \\ \cdots & \cdots & \cdots & \cdots & \cdots & \cdots \\ [\cdot]_{1\times3} & [\cdot]_{1\times3} & [0]_{1\times1} & [0]_{1\times1} & \cdots & [\cdot]_{1\times1} \end{bmatrix} \begin{bmatrix} \ddot{\boldsymbol{r}}_{B/N} \\ \dot{\boldsymbol{\omega}}_{\mathcal{B}/\mathcal{N}} \\ \ddot{\alpha}_1 \\ \ddot{\alpha}_2 \\ \cdots \\ \ddot{\alpha}_M \end{bmatrix} = \begin{bmatrix} [\cdot]_{3\times1} \\ [\cdot]_{3\times1} \\ [\cdot]_{1\times1} \\ [\cdot]_{1\times1} \\ \cdots \\ [\cdot]_{1\times1} \end{bmatrix} \tag{1}$$

where $\ddot{\boldsymbol{r}}_{B/N}$ is the hub inertial translational acceleration and $\dot{\boldsymbol{\omega}}_{\mathcal{B}/\mathcal{N}}$ is the hub inertial angular acceleration. The additional degrees of freedom required for the attached subcomponents are generalized as $\ddot{\alpha}$. M denotes the total number of additional degrees of freedom contributed by all subcomponents.

Inspection of the system mass matrix reveals a useful insight: the hub second-order state variables are coupled with all of the subcomponent second-order states and vice-versa; however, the second-order states of the subcomponents are not coupled together. Therefore, a block-diagonal form is observed for the component-on-component associations and the equations for each subcomponent can be individually expressed as

$$[\ddot{\boldsymbol{\alpha}}] = [\boldsymbol{A}_\alpha]\ddot{\boldsymbol{r}}_{B/N} + [\boldsymbol{B}_\alpha]\dot{\boldsymbol{\omega}}_{\mathcal{B}/\mathcal{N}} + [\boldsymbol{C}_\alpha] \tag{2}$$

where the $[\boldsymbol{A}_\alpha]$ and $[\boldsymbol{B}_\alpha]$ matrices contain the coupling terms between the subcomponents and the hub and the $[\boldsymbol{C}_\alpha]$ matrix contains the remaining terms. Substituting the subcomponent accelerations back into the hub equations of motion yields the condensed result where the subcomponent accelerations are decoupled from the hub accelerations

$$\begin{bmatrix} [A] & [B] \\ [C] & [D] \end{bmatrix} \begin{bmatrix} \ddot{\boldsymbol{r}}_{B/N} \\ \dot{\boldsymbol{\omega}}_{\mathcal{B}/\mathcal{N}} \end{bmatrix} = \begin{bmatrix} \boldsymbol{v}_{\text{trans}} \\ \boldsymbol{v}_{\text{rot}} \end{bmatrix} \tag{3}$$

Finally, the hub accelerations can be directly solved using Eqs. (4) and (5), where using Schur decomposition, only two 3×3 matrix inversions are required.[39]

$$\dot{\boldsymbol{\omega}}_{\mathcal{B}/\mathcal{N}} = \left([D] - [C][A]^{-1}[B]\right)^{-1} \left(\boldsymbol{v}_{\text{rot}} - [C][A]^{-1}\boldsymbol{v}_{\text{trans}}\right) \tag{4}$$

$$\ddot{\boldsymbol{r}}_{B/N} = [A]^{-1} \left(\boldsymbol{v}_{\text{trans}} - [B]\dot{\boldsymbol{\omega}}_{\mathcal{B}/\mathcal{N}}\right) \tag{5}$$

Substituting the hub accelerations back into Eq. (2) provides the accelerations for each subcomponent. The system can be numerically integrated using these results.

PROBLEM STATEMENT

Figure (2) illustrates the multibody chained system of interest for the derivation in this work. The chained system includes a rigid hub (gray), a prescribed motion component (green), and a general six-degree-of-freedom rigid body (orange).

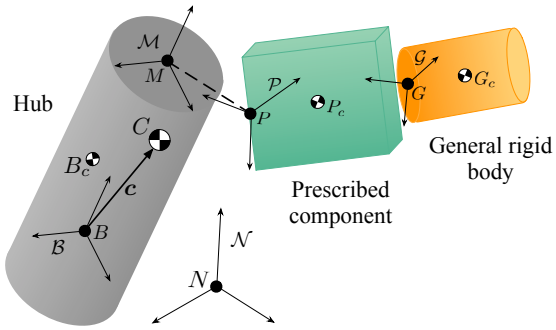

Figure 2. Problem statement for the general chained system.

Five reference frames are required to derive system dynamics. First, an inertial frame indicated by $\mathcal{N} : \{N, \hat{\boldsymbol{n}}_1, \hat{\boldsymbol{n}}_2, \hat{\boldsymbol{n}}_3\}$ is used as the base of reference for the dynamics. The motion of the rigid hub is described using the frame $\mathcal{B} : \{B, \hat{\boldsymbol{b}}_1, \hat{\boldsymbol{b}}_2, \hat{\boldsymbol{b}}_3\}$, while the motion of the prescribed and general body are defined using the frames $\mathcal{P} : \{P, \hat{\boldsymbol{p}}_1, \hat{\boldsymbol{p}}_2, \hat{\boldsymbol{p}}_3\}$ and $\mathcal{G} : \{G, \hat{\boldsymbol{g}}_1, \hat{\boldsymbol{g}}_2, \hat{\boldsymbol{g}}_3\}$, respectively. The prescribed body motion is profiled relative to a hub-fixed mount frame given by $\mathcal{M} : \{M, \hat{\boldsymbol{m}}_1, \hat{\boldsymbol{m}}_2, \hat{\boldsymbol{m}}_3\}$. This frame is introduced as a matter of kinematic convenience for development of the prescribed motion. The origin points of these frames are given by N, B, M, P, and G, respectively. The masses of the system bodies are defined as $m_{\text{hub}}, m_{\text{P}}$, and m_{G}. Finally, the center of mass points of each body are indicated by B_c, P_c, and G_c.

The translational and rotational states required to profile the prescribed component motion are given by $\boldsymbol{r}_{P/M}, \boldsymbol{r}'_{P/M}, \boldsymbol{r}''_{P/M}, \boldsymbol{\sigma}_{\mathcal{P}/\mathcal{M}}, \boldsymbol{\omega}_{\mathcal{P}/\mathcal{M}}$ and $\boldsymbol{\omega}'_{\mathcal{P}/\mathcal{M}}$. The right $'$ superscript indicates a hub $\mathcal{B}$ frame-relative time derivative. Modified Rodriguez Parameter attitude coordinates[31] are selected to express the relative orientations between reference frames.

JOINT MAPS

The motion of the general rigid body illustrated in Fig. 2 can be described using a six degree-of-freedom joint. The general vector $\boldsymbol{\beta}$ of size $N \times 1$ is used to define the degrees of freedom of

the general body relative to the prescribed component. A mapping matrix $[T]$ of size $6 \times N$ is used to map the N degrees of freedom of the general body to its vector states relative to the prescribed component. Equation 6 describes how the joint mapping matrix and degree-of-freedom vector is used to obtain the general body's velocity vectors relative to the prescribed component.

$$\begin{bmatrix} {}^{P}\frac{\mathrm{d}}{\mathrm{d}t}\boldsymbol{r}_{G/P} \\ \boldsymbol{\omega}_{\mathcal{G}/\mathcal{P}} \end{bmatrix}_{6\times 1} = \underbrace{\begin{bmatrix} T \end{bmatrix}}_{6\times N} \underbrace{\begin{bmatrix} \dot{\boldsymbol{\beta}} \end{bmatrix}}_{N\times 1} \tag{6}$$

For example, a rigid body modeled as a 1 degree-of-freedom revolute joint has the mapping matrix $[T] = \begin{bmatrix} \mathbf{0} \\ \hat{\boldsymbol{g}}_\theta \end{bmatrix}$ and degree-of-freedom vector $\boldsymbol{\beta} = [\theta]$. Table (1) provides several simple joint types and their corresponding mapping matrices and degree-of-freedom vectors.

Joint	DOF	$[T]$	$\boldsymbol{\beta}$
Revolute	1	$\begin{bmatrix} \mathbf{0} \\ \hat{\boldsymbol{g}}_\theta \end{bmatrix}$	$[\theta]$
Prismatic	1	$\begin{bmatrix} \hat{\boldsymbol{g}}_\rho \\ \mathbf{0} \end{bmatrix}$	$[\rho]$
Helical Screw	1	$\begin{bmatrix} c\hat{\boldsymbol{g}}_\theta \\ \hat{\boldsymbol{g}}_\theta \end{bmatrix}$	$[\theta]$
Cylindrical	2	$\begin{bmatrix} \hat{\boldsymbol{g}}_\rho & \mathbf{0} \\ \mathbf{0} & \hat{\boldsymbol{g}}_\theta \end{bmatrix}$	$\begin{bmatrix} \rho \\ \theta \end{bmatrix}$

Table 1. Joint types.

Joint Kinematics

Next, the general body kinematics relative to the prescribed component can be defined using the joint mapping formulation given by Eq. (6)

$$\boldsymbol{\omega}_{\mathcal{G}/\mathcal{P}} = [\Phi_\theta][T]\dot{\boldsymbol{\beta}} \tag{7}$$

$${}^{\mathcal{P}}\frac{\mathrm{d}}{\mathrm{d}t}\boldsymbol{\omega}_{\mathcal{G}/\mathcal{P}} = [\Phi_\theta][T]\ddot{\boldsymbol{\beta}} \tag{8}$$

$$\begin{aligned} \boldsymbol{r}_{G_c/P} &= \boldsymbol{r}_{G_c/G} + \boldsymbol{r}_{G/P} \\ &= \boldsymbol{r}_{G_c/G} + [\Phi_\rho][T]\boldsymbol{\beta} \end{aligned} \tag{9}$$

$$\begin{aligned} {}^{\mathcal{P}}\frac{\mathrm{d}}{\mathrm{d}t}\boldsymbol{r}_{G_c/P} &= [\tilde{\boldsymbol{\omega}}_{\mathcal{G}/\mathcal{P}}]\boldsymbol{r}_{G_c/G} + {}^{\mathcal{P}}\frac{\mathrm{d}}{\mathrm{d}t}\boldsymbol{r}_{G/P} \\ &= \left([\Phi_\rho] - \left[\tilde{\boldsymbol{r}}_{G_c/G}\right][\Phi_\theta]\right)[T]\dot{\boldsymbol{\beta}} \end{aligned} \tag{10}$$

$$\frac{^{\mathcal{P}}\mathrm{d}^2}{\mathrm{d}t^2}\boldsymbol{r}_{G_c/P} = \left([\frac{^{\mathcal{P}}\mathrm{d}}{\mathrm{d}t}\tilde{\boldsymbol{\omega}}_{\mathcal{G}/\mathcal{P}}] + [\tilde{\boldsymbol{\omega}}_{\mathcal{G}/\mathcal{P}}]^2\right)\boldsymbol{r}_{G_c/G} + \frac{^{\mathcal{P}}\mathrm{d}^2}{\mathrm{d}t^2}\boldsymbol{r}_{G/P}$$
$$= \left([\Phi_\rho] - \left[\tilde{\boldsymbol{r}}_{G_c/G}\right][\Phi_\theta]\right)[T]\ddot{\boldsymbol{\beta}} + \left[\widetilde{[\Phi_\theta][T]\dot{\boldsymbol{\beta}}}\right]^2\boldsymbol{r}_{G_c/G} \tag{11}$$

where $[\Phi_\rho] = \begin{bmatrix}[I]_{3\times3} & [\mathbf{0}]_{3\times3}\end{bmatrix}$ and $[\Phi_\theta] = \begin{bmatrix}[\mathbf{0}]_{3\times3} & [I]_{3\times3}\end{bmatrix}$.

EQUATIONS OF MOTION DERIVATION

This section derives the general equations of motion for the three-body chained system containing a rigid hub, intermediate prescribed motion component, and a six-degree-of-freedom general rigid body. Newtonian and Eulerian mechanics are used for the equation-of-motion development. Moreover, note that that while the presented derivation considers only a single rigid body attached to the prescribed component, the results are immediately scalable for N single-body attachments.

System Translational Equations of Motion

The spacecraft hub translational equations of motion define the first three system degrees of freedom. These equations are derived starting from Newton's Second Law for the spacecraft center of mass[?]

$$m_{\text{sc}}\ddot{\boldsymbol{r}}_{C/N} = m_{\text{sc}}\ddot{\boldsymbol{c}} + m_{\text{sc}}\ddot{\boldsymbol{r}}_{B/N} = \sum \boldsymbol{F}_{\text{ext}} \tag{12}$$

where m_{sc} is the total mass of the spacecraft system, $m_{\text{sc}} = m_{\text{hub}} + m_{\text{P}} + m_{\text{G}}$, and $\sum \boldsymbol{F}_{\text{ext}}$ is the sum of all external forces acting on the system. Note that because the hub equations of motion are of interest for this formulation, the acceleration of the hub frame origin point B must be defined. First, the transport theorem[?] is used to relate the hub-relative derivative of the center of mass vector to its inertial time derivative

$$\dot{\boldsymbol{c}} = \boldsymbol{c}' + \boldsymbol{\omega}_{\mathcal{B}/\mathcal{N}} \times \boldsymbol{c} \tag{13}$$
$$\ddot{\boldsymbol{c}} = \boldsymbol{c}'' + 2\boldsymbol{\omega}_{\mathcal{B}/\mathcal{N}} \times \boldsymbol{c}' + \dot{\boldsymbol{\omega}}_{\mathcal{B}/\mathcal{N}} \times \boldsymbol{c} + \boldsymbol{\omega}_{\mathcal{B}/\mathcal{N}} \times \boldsymbol{\omega}_{\mathcal{B}/\mathcal{N}} \times \boldsymbol{c} \tag{14}$$

The system center of mass vector is defined using the mass contributions from all of the system bodies

$$\boldsymbol{c} = \frac{m_{\text{hub}}\boldsymbol{r}_{B_c/B} + m_{\text{P}}\boldsymbol{r}_{P_c/B} + m_{\text{G}}\boldsymbol{r}_{G_c/B}}{m_{\text{sc}}} \tag{15}$$

The hub-relative velocity of the center of mass vector is

$$\boldsymbol{c}' = \frac{m_{\text{P}}\boldsymbol{r}'_{P_c/B} + m_{\text{G}}\boldsymbol{r}'_{G_c/B}}{m_{\text{sc}}} \tag{16}$$

where using the transport theorem yields

$$\boldsymbol{r}'_{P_c/B} = \boldsymbol{r}'_{P_c/P} + \boldsymbol{r}'_{P/M} + \boldsymbol{r}'_{M/B} = \boldsymbol{\omega}_{\mathcal{P}/\mathcal{B}} \times \boldsymbol{r}_{P_c/P} + \boldsymbol{r}'_{P/M} \tag{17}$$
$$\boldsymbol{r}'_{G_c/B} = \boldsymbol{r}'_{G_c/P} + \boldsymbol{r}'_{P/B} = \frac{^{\mathcal{P}}\mathrm{d}}{\mathrm{d}t}\boldsymbol{r}_{G_c/P} + \boldsymbol{\omega}_{\mathcal{P}/\mathcal{B}} \times \boldsymbol{r}_{G_c/P} + \boldsymbol{r}'_{P/B} \tag{18}$$

Similarly, the hub-relative acceleration of the center of mass vector is

$$\boldsymbol{c}'' = \frac{m_{\text{P}}\boldsymbol{r}''_{P_c/B} + m_{\text{G}}\boldsymbol{r}''_{G_c/B}}{m_{\text{sc}}} \tag{19}$$

where

$$\boldsymbol{r}''_{P_c/B} = \left([\tilde{\boldsymbol{\omega}}'_{\mathcal{P}/\mathcal{B}}] + [\tilde{\boldsymbol{\omega}}_{\mathcal{P}/\mathcal{B}}]^2\right)\boldsymbol{r}_{P_c/P} + \boldsymbol{r}''_{P/B} \tag{20}$$

$$\boldsymbol{r}''_{G_c/B} = \frac{^{\mathcal{P}}\mathrm{d}^2}{\mathrm{d}t^2}\boldsymbol{r}_{G_c/P} + 2[\tilde{\boldsymbol{\omega}}_{\mathcal{P}/\mathcal{B}}]\frac{^{\mathcal{P}}\mathrm{d}}{\mathrm{d}t}\boldsymbol{r}_{G_c/P} + \left([\tilde{\boldsymbol{\omega}}'_{\mathcal{P}/\mathcal{B}}] + [\tilde{\boldsymbol{\omega}}_{\mathcal{P}/\mathcal{B}}]^2\right)\boldsymbol{r}_{G_c/P} + \boldsymbol{r}''_{P/B} \tag{21}$$

Substituting Eqs. (14) and (19) into Eq. (12) yields a compact expression for the system translational equations of motion

$$m_{\mathrm{sc}}\ddot{\boldsymbol{r}}_{B/N} + m_{\mathrm{sc}}[\dot{\tilde{\boldsymbol{\omega}}}_{\mathcal{B}/\mathcal{N}}]\boldsymbol{c} = \sum \boldsymbol{F}_{\mathrm{ext}} - 2m_{\mathrm{sc}}[\tilde{\boldsymbol{\omega}}_{\mathcal{B}/\mathcal{N}}]\boldsymbol{c}' - m_{\mathrm{sc}}[\tilde{\boldsymbol{\omega}}_{\mathcal{B}/\mathcal{N}}]^2\boldsymbol{c} - m_{\mathrm{P}}\boldsymbol{r}''_{P_c/B} - m_{\mathrm{G}}\boldsymbol{r}''_{G_c/B} \tag{22}$$

Note that the above equation does not explicitly reveal the coupling between the general rigid body and the prescribed body. As written, this equation is equally valid for describing a system where both bodies are directly attached to the hub. Substituting Eq. (21) into Eq. (22) yields an expanded form that exposes the coupling terms required to simulate this specific chained system

$$\begin{aligned} m_{\mathrm{sc}}\ddot{\boldsymbol{r}}_{B/N} + m_{\mathrm{sc}}[\dot{\tilde{\boldsymbol{\omega}}}_{\mathcal{B}/\mathcal{N}}]\boldsymbol{c} &= \sum \boldsymbol{F}_{\mathrm{ext}} - 2m_{\mathrm{sc}}[\tilde{\boldsymbol{\omega}}_{\mathcal{B}/\mathcal{N}}]\boldsymbol{c}' - m_{\mathrm{sc}}[\tilde{\boldsymbol{\omega}}_{\mathcal{B}/\mathcal{N}}]^2\boldsymbol{c} \\ \text{Prescribed and general body contributions} &\left\{ -m_{\mathrm{P}}\boldsymbol{r}''_{P_c/B} - m_{\mathrm{G}}\frac{^{\mathcal{P}}\mathrm{d}^2}{\mathrm{d}t^2}\boldsymbol{r}_{G_c/P} \right. \\ \text{Coupling contr.} &\left\{ -m_{\mathrm{G}}\left(2[\tilde{\boldsymbol{\omega}}_{\mathcal{P}/\mathcal{B}}]\frac{^{\mathcal{P}}\mathrm{d}}{\mathrm{d}t}\boldsymbol{r}_{G_c/P} + \left([\tilde{\boldsymbol{\omega}}'_{\mathcal{P}/\mathcal{B}}] + [\tilde{\boldsymbol{\omega}}_{\mathcal{P}/\mathcal{B}}]^2\right)\boldsymbol{r}_{G_c/P} + \boldsymbol{r}''_{P/B}\right) \right. \end{aligned} \tag{23}$$

The coupling terms required to simulate the chained system in this work are seen in the third line of Eq. (23). Indeed, if the prescribed body is removed from the system, Eq. (23) collapses and yields Eq. (22).

Finally, generalizing Eq. (23) using the general body joint map kinematics given in the previous section gives the final form for the hub translational equations of motion

$$\begin{aligned} &m_{\mathrm{sc}}\ddot{\boldsymbol{r}}_{B/N} + m_{\mathrm{sc}}[\dot{\tilde{\boldsymbol{\omega}}}_{\mathcal{B}/\mathcal{N}}]\boldsymbol{c} + m_{\mathrm{G}}\left([\Phi_\rho] - \left[\tilde{\boldsymbol{r}}_{G_c/G}\right][\Phi_\theta]\right)[T]\ddot{\boldsymbol{\beta}} = \\ &\quad \sum \boldsymbol{F}_{\mathrm{ext}} - 2m_{\mathrm{sc}}[\tilde{\boldsymbol{\omega}}_{\mathcal{B}/\mathcal{N}}]\boldsymbol{c}' - m_{\mathrm{sc}}[\tilde{\boldsymbol{\omega}}_{\mathcal{B}/\mathcal{N}}]^2\boldsymbol{c} \\ &\quad \text{Prescribed and general body contr.} \left\{ -m_{\mathrm{P}}\boldsymbol{r}''_{P_c/B} - m_{\mathrm{G}}\left[\widetilde{[\Phi_\theta][T]\dot{\boldsymbol{\beta}}}\right]^2\boldsymbol{r}_{G_c/G} \right. \\ &\quad \text{Coupling contr.} \left\{ \begin{array}{l} -m_{\mathrm{G}}\left(2[\tilde{\boldsymbol{\omega}}_{\mathcal{P}/\mathcal{B}}]\left([\Phi_\rho] - \left[\tilde{\boldsymbol{r}}_{G_c/G}\right][\Phi_\theta]\right)[T]\dot{\boldsymbol{\beta}}\right. \\ \left. + \left([\tilde{\boldsymbol{\omega}}'_{\mathcal{P}/\mathcal{B}}] + [\tilde{\boldsymbol{\omega}}_{\mathcal{P}/\mathcal{B}}]^2\right)\left(\boldsymbol{r}_{G_c/G} + [\Phi_\rho][T]\boldsymbol{\beta}\right) + \boldsymbol{r}''_{P/B}\right) \end{array} \right. \end{aligned} \tag{24}$$

System Rotational Equations of Motion

The spacecraft hub rotational equations of motion describe the three remaining hub degrees of freedom. The derivation begins by applying Euler's equation to the case where the spacecraft angular momentum is expressed about a hub-fixed point not coincident with the system center of mass[?]

$$\dot{\boldsymbol{H}}_{\mathrm{sc},B} = \sum \boldsymbol{L}_B + m_{\mathrm{sc}}\ddot{\boldsymbol{r}}_{B/N} \times \boldsymbol{c} \tag{25}$$

where $\boldsymbol{H}_{\text{sc},B}$ is the inertial angular momentum of the spacecraft system about point B and $\sum \boldsymbol{L}_B$ is the total external torque acting on the system about point B. First, the system angular momentum about point B is

$$\begin{aligned}\boldsymbol{H}_{\text{sc},B} = \boldsymbol{H}_{\text{hub},B} + \boldsymbol{H}_{\text{P},B} + \boldsymbol{H}_{\text{G},B} = &\left([I_{\text{hub},B}] + [I_{\text{P},B}] + [I_{\text{G},B}]\right)\boldsymbol{\omega}_{\mathcal{B}/\mathcal{N}} \\ &+ [I_{\text{P},P_c}]\boldsymbol{\omega}_{\mathcal{P}/\mathcal{B}} + m_{\text{P}}[\tilde{\boldsymbol{r}}_{P_c/B}]\boldsymbol{r}'_{P_c/B} \\ &+ [I_{\text{G},G_c}]\boldsymbol{\omega}_{\mathcal{G}/\mathcal{B}} + m_{\text{G}}[\tilde{\boldsymbol{r}}_{G_c/B}]\boldsymbol{r}'_{G_c/B}\end{aligned} \tag{26}$$

where $[I_{\text{hub},B}], [I_{\text{P},B}]$, and $[I_{\text{G},B}]$ are the hub, prescribed, and general body inertia tensors about point B. $[I_{\text{P},P_c}]$ and $[I_{\text{G},G_c}]$ are the prescribed and general body inertia tensors about their centers of mass. Combining all inertia tensors about point B yields the total spacecraft inertia about point B

$$[I_{\text{sc},B}] = [I_{\text{hub},B}] + [I_{\text{P},B}] + [I_{\text{G},B}] \tag{27}$$

Simplifying reduces Eq. (26) to

$$\begin{aligned}\boldsymbol{H}_{\text{sc},B} = &[I_{\text{sc},B}]\boldsymbol{\omega}_{\mathcal{B}/\mathcal{N}} + [I_{\text{P},P_c}]\boldsymbol{\omega}_{\mathcal{P}/\mathcal{B}} + m_{\text{P}}[\tilde{\boldsymbol{r}}_{P_c/B}]\boldsymbol{r}'_{P_c/B} \\ &+ [I_{\text{G},G_c}]\boldsymbol{\omega}_{\mathcal{G}/\mathcal{B}} + m_{\text{G}}[\tilde{\boldsymbol{r}}_{G_c/B}]\boldsymbol{r}'_{G_c/B}\end{aligned} \tag{28}$$

Next, the inertial time derivative of the total spacecraft angular momentum is expressed using the transport theorem as

$$\begin{aligned}\dot{\boldsymbol{H}}_{\text{sc},B} = &[I'_{\text{sc},B}]\boldsymbol{\omega}_{\mathcal{B}/\mathcal{N}} + [I_{\text{sc},B}]\dot{\boldsymbol{\omega}}_{\mathcal{B}/\mathcal{N}} \\ &+ [I_{\text{P},P_c}]\boldsymbol{\omega}'_{\mathcal{P}/\mathcal{B}} + [\tilde{\boldsymbol{\omega}}_{\mathcal{P}/\mathcal{N}}][I_{\text{P},P_c}]\boldsymbol{\omega}_{\mathcal{P}/\mathcal{B}} + m_{\text{P}}[\tilde{\boldsymbol{r}}_{P_c/B}]\boldsymbol{r}''_{P_c/B} + m_{\text{P}}[\tilde{\boldsymbol{\omega}}_{\mathcal{B}/\mathcal{N}}][\tilde{\boldsymbol{r}}_{P_c/B}]\boldsymbol{r}'_{P_c/B} \\ &+ [I_{\text{G},G_c}]\boldsymbol{\omega}'_{\mathcal{G}/\mathcal{B}} + [\tilde{\boldsymbol{\omega}}_{\mathcal{G}/\mathcal{N}}][I_{\text{G},G_c}]\boldsymbol{\omega}_{\mathcal{G}/\mathcal{B}} + m_{\text{G}}[\tilde{\boldsymbol{r}}_{G_c/B}]\boldsymbol{r}''_{G_c/B} + m_{\text{G}}[\tilde{\boldsymbol{\omega}}_{\mathcal{B}/\mathcal{N}}][\tilde{\boldsymbol{r}}_{G_c/B}]\boldsymbol{r}'_{G_c/B}\end{aligned} \tag{29}$$

Using the rigid body assumption for the hub and the parallel axis theorem to express the subcomponent inertias about point B yields the $\mathcal{B}$ frame derivative of the spacecraft inertia tensor

$$\begin{aligned}[I'_{\text{sc},B}] = [I'_{\text{P},B}] + [I'_{\text{G},B}] \ = &\left([I'_{\text{P},P_c}] + m_{\text{P}}\left([\tilde{\boldsymbol{r}}'_{P_c/B}][\tilde{\boldsymbol{r}}_{P_c/B}]^T + [\tilde{\boldsymbol{r}}_{P_c/B}][\tilde{\boldsymbol{r}}'_{P_c/B}]^T\right)\right) \\ &+ \left([I'_{\text{G},G_c}] + m_{\text{G}}\left([\tilde{\boldsymbol{r}}'_{G_c/B}][\tilde{\boldsymbol{r}}_{G_c/B}]^T + [\tilde{\boldsymbol{r}}_{G_c/B}][\tilde{\boldsymbol{r}}'_{G_c/B}]^T\right)\right)\end{aligned} \tag{30}$$

The inertia transport theorem[?] is used to express the subcomponent inertias about their centers of mass

$$[I'_{\text{P},P_c}] = [\tilde{\boldsymbol{\omega}}_{\mathcal{P}/\mathcal{B}}][I_{\text{P},P_c}] - [I_{\text{P},P_c}][\tilde{\boldsymbol{\omega}}_{\mathcal{P}/\mathcal{B}}] \tag{31}$$

$$[I'_{\text{G},G_c}] = [\tilde{\boldsymbol{\omega}}_{\mathcal{G}/\mathcal{B}}][I_{\text{G},G_c}] - [I_{\text{G},G_c}][\tilde{\boldsymbol{\omega}}_{\mathcal{G}/\mathcal{B}}] \tag{32}$$

Equation (30) then becomes

$$\begin{aligned}[I'_{\text{sc},B}] = &\left([\tilde{\boldsymbol{\omega}}_{\mathcal{P}/\mathcal{B}}][I_{\text{P},P_c}] - [I_{\text{P},P_c}][\tilde{\boldsymbol{\omega}}_{\mathcal{P}/\mathcal{B}}] + m_{\text{P}}\left([\tilde{\boldsymbol{r}}'_{P_c/B}][\tilde{\boldsymbol{r}}_{P_c/B}]^T + [\tilde{\boldsymbol{r}}_{P_c/B}][\tilde{\boldsymbol{r}}'_{P_c/B}]^T\right)\right) \\ &+ \left([\tilde{\boldsymbol{\omega}}_{\mathcal{G}/\mathcal{B}}][I_{\text{G},G_c}] - [I_{\text{G},G_c}][\tilde{\boldsymbol{\omega}}_{\mathcal{G}/\mathcal{B}}] + m_{\text{G}}\left([\tilde{\boldsymbol{r}}'_{G_c/B}][\tilde{\boldsymbol{r}}_{G_c/B}]^T + [\tilde{\boldsymbol{r}}_{G_c/B}][\tilde{\boldsymbol{r}}'_{G_c/B}]^T\right)\right)\end{aligned} \tag{33}$$

Combining these results and arranging the terms in the form of the backsubstitution method yields the system rotational equations of motion

$$
\begin{aligned}
m_{\mathrm{sc}}[\tilde{\boldsymbol{c}}]\ddot{\boldsymbol{r}}_{B/N} + [I_{\mathrm{sc},B}]\dot{\boldsymbol{\omega}}_{\mathcal{B}/\mathcal{N}} = \sum \boldsymbol{L}_B - \left([I'_{\mathrm{sc},B}] + [\tilde{\boldsymbol{\omega}}_{\mathcal{B}/\mathcal{N}}][I_{\mathrm{sc},B}]\right)\boldsymbol{\omega}_{\mathcal{B}/\mathcal{N}} \\
- \left([I_{\mathrm{P},P_c}]\boldsymbol{\omega}'_{\mathcal{P}/\mathcal{B}} + m_{\mathrm{P}}[\tilde{\boldsymbol{r}}_{P_c/B}]\boldsymbol{r}''_{P_c/B} + [\tilde{\boldsymbol{\omega}}_{\mathcal{P}/\mathcal{N}}][I_{\mathrm{P},P_c}]\boldsymbol{\omega}_{\mathcal{P}/\mathcal{B}} + m_{\mathrm{P}}[\tilde{\boldsymbol{\omega}}_{\mathcal{B}/\mathcal{N}}][\tilde{\boldsymbol{r}}_{P_c/B}]\boldsymbol{r}'_{P_c/B}\right) \\
- \left([I_{\mathrm{G},G_c}]\boldsymbol{\omega}'_{\mathcal{G}/\mathcal{B}} + m_{\mathrm{G}}[\tilde{\boldsymbol{r}}_{G_c/B}]\boldsymbol{r}''_{G_c/B} + [\tilde{\boldsymbol{\omega}}_{\mathcal{G}/\mathcal{N}}][I_{\mathrm{G},G_c}]\boldsymbol{\omega}_{\mathcal{G}/\mathcal{B}} + m_{\mathrm{G}}[\tilde{\boldsymbol{\omega}}_{\mathcal{B}/\mathcal{N}}][\tilde{\boldsymbol{r}}_{G_c/B}]\boldsymbol{r}'_{G_c/B}\right)
\end{aligned}
\tag{34}
$$

Similar to the translational equations of motion, note that Eq. (34) does not expose the coupling terms associated with the chain of bodies studied in this work. The expanded translational terms are given in Eqs. (18) and (21). The following terms must also be expanded

$$
\boldsymbol{\omega}_{\mathcal{B}/\mathcal{N}} = \boldsymbol{\omega}_{\mathcal{P}/\mathcal{N}} - \boldsymbol{\omega}_{\mathcal{P}/\mathcal{B}} \tag{35}
$$

$$
\boldsymbol{\omega}_{\mathcal{G}/\mathcal{B}} = \boldsymbol{\omega}_{\mathcal{G}/\mathcal{P}} + \boldsymbol{\omega}_{\mathcal{P}/\mathcal{B}} \tag{36}
$$

$$
\boldsymbol{\omega}'_{\mathcal{G}/\mathcal{B}} = \frac{{}^{\mathcal{P}}\mathrm{d}}{\mathrm{d}t}\boldsymbol{\omega}_{\mathcal{G}/\mathcal{P}} + \boldsymbol{\omega}'_{\mathcal{P}/\mathcal{B}} \tag{37}
$$

Substituting these results into Eq. (34) yields the expanded form

$$
\begin{aligned}
&m_{\mathrm{sc}}[\tilde{\boldsymbol{c}}]\ddot{\boldsymbol{r}}_{B/N} + [I_{\mathrm{sc},B}]\dot{\boldsymbol{\omega}}_{\mathcal{B}/\mathcal{N}} = \sum \boldsymbol{L}_B - \left([I'_{\mathrm{sc},B}] + [\tilde{\boldsymbol{\omega}}_{\mathcal{B}/\mathcal{N}}][I_{\mathrm{sc},B}]\right)\boldsymbol{\omega}_{\mathcal{B}/\mathcal{N}} \\
&\text{Prescribed contributions} \begin{cases} - [I_{\mathrm{P},P_c}]\boldsymbol{\omega}'_{\mathcal{P}/\mathcal{B}} - m_{\mathrm{P}}[\tilde{\boldsymbol{r}}_{P_c/B}]\boldsymbol{r}''_{P_c/B} \\ - [\tilde{\boldsymbol{\omega}}_{\mathcal{P}/\mathcal{N}}][I_{\mathrm{P},P_c}]\boldsymbol{\omega}_{\mathcal{P}/\mathcal{B}} - m_{\mathrm{P}}[\tilde{\boldsymbol{\omega}}_{\mathcal{B}/\mathcal{N}}][\tilde{\boldsymbol{r}}_{P_c/B}]\boldsymbol{r}'_{P_c/B} \end{cases} \\
&\text{General body contributions} \begin{cases} - [I_{\mathrm{G},G_c}]\dfrac{{}^{\mathcal{P}}\mathrm{d}}{\mathrm{d}t}\boldsymbol{\omega}_{\mathcal{G}/\mathcal{P}} - m_{\mathrm{G}}[\tilde{\boldsymbol{r}}_{G_c/P}]\dfrac{{}^{\mathcal{P}}\mathrm{d}^2}{\mathrm{d}t^2}\boldsymbol{r}_{G_c/P} \\ - [\tilde{\boldsymbol{\omega}}_{\mathcal{G}/\mathcal{N}}][I_{\mathrm{G},G_c}]\boldsymbol{\omega}_{\mathcal{G}/\mathcal{P}} - m_{\mathrm{G}}[\tilde{\boldsymbol{\omega}}_{\mathcal{P}/\mathcal{N}}][\tilde{\boldsymbol{r}}_{G_c/P}]\dfrac{{}^{\mathcal{P}}\mathrm{d}}{\mathrm{d}t}\boldsymbol{r}_{G_c/P} \end{cases} \\
&\text{Coupling contr.} \begin{cases} - [I_{\mathrm{G},G_c}]\left([\tilde{\boldsymbol{\omega}}_{\mathcal{P}/\mathcal{B}}]\boldsymbol{\omega}_{\mathcal{G}/\mathcal{P}} + \boldsymbol{\omega}'_{\mathcal{P}/\mathcal{B}}\right) - [\tilde{\boldsymbol{\omega}}_{\mathcal{G}/\mathcal{N}}][I_{\mathrm{G},G_c}]\boldsymbol{\omega}_{\mathcal{P}/\mathcal{B}} \\ - m_{\mathrm{G}}[\tilde{\boldsymbol{r}}_{P/B}]\dfrac{{}^{\mathcal{P}}\mathrm{d}^2}{\mathrm{d}t^2}\boldsymbol{r}_{G_c/P} \\ - m_{\mathrm{G}}[\tilde{\boldsymbol{r}}_{G_c/B}]\left(2[\tilde{\boldsymbol{\omega}}_{\mathcal{P}/\mathcal{B}}]\dfrac{{}^{\mathcal{P}}\mathrm{d}}{\mathrm{d}t}\boldsymbol{r}_{G_c/P} + \left([\tilde{\boldsymbol{\omega}}'_{\mathcal{P}/\mathcal{B}}] + [\tilde{\boldsymbol{\omega}}_{\mathcal{P}/\mathcal{B}}]^2\right)\boldsymbol{r}_{G_c/P} + \boldsymbol{r}''_{P/B}\right) \\ - m_{\mathrm{G}}\left([\tilde{\boldsymbol{\omega}}_{\mathcal{B}/\mathcal{N}}][\tilde{\boldsymbol{r}}_{P/B}] - [\tilde{\boldsymbol{\omega}}_{\mathcal{P}/\mathcal{B}}][\tilde{\boldsymbol{r}}_{G_c/P}]\right)\dfrac{{}^{\mathcal{P}}\mathrm{d}}{\mathrm{d}t}\boldsymbol{r}_{G_c/P} \\ - m_{\mathrm{G}}[\tilde{\boldsymbol{\omega}}_{\mathcal{B}/\mathcal{N}}][\tilde{\boldsymbol{r}}_{G_c/B}]\left([\tilde{\boldsymbol{\omega}}_{\mathcal{P}/\mathcal{B}}]\boldsymbol{r}_{G_c/P} + \boldsymbol{r}'_{P/B}\right) \end{cases}
\end{aligned}
\tag{38}
$$

The coupling terms required to simulate the chained system in this work are grouped at the end of Eq. (38). Indeed, if the prescribed body is removed from the system, Eq. (38) collapses and yields Eq. (34).

Finally, generalizing Eq. (38) using the general body joint map kinematics gives the final form for the hub rotational equations of motion

$$
m_{\mathrm{sc}}[\tilde{\boldsymbol{c}}]\ddot{\boldsymbol{r}}_{B/N} + [I_{\mathrm{sc},B}]\dot{\boldsymbol{\omega}}_{\mathcal{B}/\mathcal{N}}
$$

$$
\begin{aligned}
&+\left(\left[I_{\mathrm{G},G_c}\right]\left[\Phi_\theta\right]+m_{\mathrm{G}}[\boldsymbol{r}_{G_c/G}+\widetilde{[\Phi_\rho]}[T]\boldsymbol{\beta}+\boldsymbol{r}_{P/B}]\left(\left[\Phi_\rho\right]-\left[\tilde{\boldsymbol{r}}_{G_c/G}\right]\left[\Phi_\theta\right]\right)\right)[T]\ddot{\boldsymbol{\beta}}\\
&=\sum \boldsymbol{L}_B-\left(\left[I'_{\mathrm{sc},B}\right]+[\tilde{\boldsymbol{\omega}}_{\mathcal{B}/\mathcal{N}}][I_{\mathrm{sc},B}]\right)\boldsymbol{\omega}_{\mathcal{B}/\mathcal{N}}\\
&\text{Prescribed contributions}\begin{cases}-\left[I_{\mathrm{P},P_c}\right]\boldsymbol{\omega}'_{\mathcal{P}/\mathcal{B}}-m_{\mathrm{P}}[\tilde{\boldsymbol{r}}_{P_c/B}]\boldsymbol{r}''_{P_c/B}\\-[\tilde{\boldsymbol{\omega}}_{\mathcal{P}/\mathcal{N}}][I_{\mathrm{P},P_c}]\boldsymbol{\omega}_{\mathcal{P}/\mathcal{B}}-m_{\mathrm{P}}[\tilde{\boldsymbol{\omega}}_{\mathcal{B}/\mathcal{N}}][\tilde{\boldsymbol{r}}_{P_c/B}]\boldsymbol{r}'_{P_c/B}\end{cases}\\
&\text{General body contributions}\begin{cases}-m_{\mathrm{G}}[\boldsymbol{r}_{G_c/G}\widetilde{+[\Phi_\rho]}[T]\boldsymbol{\beta}]\left[\widetilde{[\Phi_\theta][T]\dot{\boldsymbol{\beta}}}\right]^2\boldsymbol{r}_{G_c/G}\\-\left[\left[\Phi_\theta\right]\widetilde{[T]\dot{\boldsymbol{\beta}}+\boldsymbol{\omega}_{\mathcal{P}/\mathcal{N}}}\right]\left[I_{\mathrm{G},G_c}\right]\left[\Phi_\theta\right][T]\dot{\boldsymbol{\beta}}\\-m_{\mathrm{G}}[\tilde{\boldsymbol{\omega}}_{\mathcal{P}/\mathcal{N}}]\left[\boldsymbol{r}_{G_c/G}\widetilde{+[\Phi_\rho]}[T]\boldsymbol{\beta}\right]\left(\left[\Phi_\rho\right]-\left[\tilde{\boldsymbol{r}}_{G_c/G}\right]\left[\Phi_\theta\right]\right)[T]\dot{\boldsymbol{\beta}}\end{cases}\\
&\text{Coupling contr.}\begin{cases}-\left[I_{\mathrm{G},G_c}\right]\left([\tilde{\boldsymbol{\omega}}_{\mathcal{P}/\mathcal{B}}]\left[\Phi_\theta\right][T]\dot{\boldsymbol{\beta}}+\boldsymbol{\omega}'_{\mathcal{P}/\mathcal{B}}\right)-\left[\left[\Phi_\theta\right]\widetilde{[T]\dot{\boldsymbol{\beta}}+\boldsymbol{\omega}_{\mathcal{P}/\mathcal{N}}}\right]\left[I_{\mathrm{G},G_c}\right]\boldsymbol{\omega}_{\mathcal{P}/\mathcal{B}}\\-m_{\mathrm{G}}[\tilde{\boldsymbol{r}}_{P/B}]\left[\widetilde{[\Phi_\theta][T]\dot{\boldsymbol{\beta}}}\right]^2\boldsymbol{r}_{G_c/G}\\-m_{\mathrm{G}}\left[\boldsymbol{r}_{G_c/G}+\widetilde{[\Phi_\rho][T]\boldsymbol{\beta}}+\boldsymbol{r}_{P/B}\right]\left(2[\tilde{\boldsymbol{\omega}}_{\mathcal{P}/\mathcal{B}}]\left(\left[\Phi_\rho\right]-\left[\tilde{\boldsymbol{r}}_{G_c/G}\right]\left[\Phi_\theta\right]\right)[T]\dot{\boldsymbol{\beta}}\right.\\+\left.\left([\tilde{\boldsymbol{\omega}}'_{\mathcal{P}/\mathcal{B}}]+[\tilde{\boldsymbol{\omega}}_{\mathcal{P}/\mathcal{B}}]^2\right)\left(\boldsymbol{r}_{G_c/G}+\left[\Phi_\rho\right][T]\boldsymbol{\beta}\right)+\boldsymbol{r}''_{P/B}\right)\\-m_{\mathrm{G}}\left([\tilde{\boldsymbol{\omega}}_{\mathcal{B}/\mathcal{N}}][\tilde{\boldsymbol{r}}_{P/B}]-[\tilde{\boldsymbol{\omega}}_{\mathcal{P}/\mathcal{B}}]\left[\boldsymbol{r}_{G_c/G}\widetilde{+[\Phi_\rho]}[T]\boldsymbol{\beta}\right]\right)\left(\left[\Phi_\rho\right]-\left[\tilde{\boldsymbol{r}}_{G_c/G}\right]\left[\Phi_\theta\right]\right)[T]\dot{\boldsymbol{\beta}}\\-m_{\mathrm{G}}[\tilde{\boldsymbol{\omega}}_{\mathcal{B}/\mathcal{N}}]\left[\boldsymbol{r}_{G_c/G}+\widetilde{[\Phi_\rho][T]\boldsymbol{\beta}}+\boldsymbol{r}_{P/B}\right]\left([\tilde{\boldsymbol{\omega}}_{\mathcal{P}/\mathcal{B}}]\left(\boldsymbol{r}_{G_c/G}+\left[\Phi_\rho\right][T]\boldsymbol{\beta}\right)+\boldsymbol{r}'_{P/B}\right)\end{cases}
\end{aligned}
\tag{39}
$$

General Body Translational Equations of Motion

The general body translational equations of motion are derived using Newton's second law

$$
m_{\mathrm{G}}\ddot{\boldsymbol{r}}_{G_c/N}=\sum \boldsymbol{F}_{\mathrm{G}} \tag{40}
$$

where

$$
\ddot{\boldsymbol{r}}_{G_c/N}=\frac{{}^{\mathcal{P}}\mathrm{d}^2}{\mathrm{d}t^2}\boldsymbol{r}_{G_c/P}+2[\tilde{\boldsymbol{\omega}}_{\mathcal{P}/\mathcal{N}}]\frac{{}^{\mathcal{P}}\mathrm{d}}{\mathrm{d}t}\boldsymbol{r}_{G_c/P}+\left([\dot{\tilde{\boldsymbol{\omega}}}_{\mathcal{P}/\mathcal{N}}]+[\tilde{\boldsymbol{\omega}}_{\mathcal{P}/\mathcal{N}}]^2\right)\boldsymbol{r}_{G_c/P}+\ddot{\boldsymbol{r}}_{P/N} \tag{41}
$$

Substitution of the general body kinematics given by Eqs. (9-11) into Eq. (41), followed by substitution of Eq. (41) into Eq. (40) yields the general body translational equations of motion

$$
\begin{aligned}
m_{\mathrm{G}}\left(\left[\Phi_\rho\right]-\left[\tilde{\boldsymbol{r}}_{G_c/G}\right]\left[\Phi_\theta\right][T]\ddot{\boldsymbol{\beta}}\right.&=-m_{\mathrm{G}}\ddot{\boldsymbol{r}}_{P/N}+m_{\mathrm{G}}\left[\boldsymbol{r}_{G_c/G}\widetilde{+[\Phi_\rho]}[T]\boldsymbol{\beta}\right]\dot{\boldsymbol{\omega}}_{\mathcal{P}/\mathcal{N}}\\
&+\sum \boldsymbol{F}_{\mathrm{G}}-2m_{\mathrm{G}}[\tilde{\boldsymbol{\omega}}_{\mathcal{P}/\mathcal{N}}]\left(\left[\Phi_\rho\right]-\left[\tilde{\boldsymbol{r}}_{G_c/G}\right]\left[\Phi_\theta\right]\right)[T]\dot{\boldsymbol{\beta}}\\
&-m_{\mathrm{G}}[\tilde{\boldsymbol{\omega}}_{\mathcal{P}/\mathcal{N}}]^2\left(\boldsymbol{r}_{G_c/G}+\left[\Phi_\rho\right][T]\boldsymbol{\beta}\right)-m_{\mathrm{G}}\left[\widetilde{[\Phi_\theta][T]\dot{\boldsymbol{\beta}}}\right]^2\boldsymbol{r}_{G_c/G}
\end{aligned}
\tag{42}
$$

General Body Rotational Equations of Motion

The general body rotational equations of motion are developed using Euler's equation

$$
\dot{\boldsymbol{H}}_{\mathrm{G},G}=\sum \boldsymbol{L}_G-m_{\mathrm{G}}[\tilde{\boldsymbol{r}}_{G_c/G}]\ddot{\boldsymbol{r}}_{G/N} \tag{43}
$$

where

$$\boldsymbol{H}_{\mathrm{G},G} = [I_{\mathrm{G},G}]\boldsymbol{\omega}_{\mathcal{G}/\mathcal{N}} \tag{44}$$

Taking the inertial time derivative of Eq. (44) gives the left-hand side of Eq. (43):

$$\begin{aligned}\dot{\boldsymbol{H}}_{\mathrm{G},G} = &\left[[\Phi_\theta][T]\dot{\boldsymbol{\beta}} + \boldsymbol{\omega}_{\mathcal{P}/\mathcal{N}}\right][I_{\mathrm{G},G}]\left([\Phi_\theta][T]\dot{\boldsymbol{\beta}} + \boldsymbol{\omega}_{\mathcal{P}/\mathcal{N}}\right)\\ &+ [I_{\mathrm{G},G}][\Phi_\theta][T]\ddot{\boldsymbol{\beta}} + [I_{\mathrm{G},G}][\tilde{\boldsymbol{\omega}}_{\mathcal{P}/\mathcal{N}}][\Phi_\theta][T]\dot{\boldsymbol{\beta}} + [I_{\mathrm{G},G}]\dot{\boldsymbol{\omega}}_{\mathcal{P}/\mathcal{N}}\end{aligned} \tag{45}$$

Substitution of Eq. (45) into Eq. (43) and expanding $\ddot{\boldsymbol{r}}_{G/N}$ gives the general body rotational equations of motion

$$\begin{aligned}([I_{\mathrm{G},G}][\Phi_\theta] + m_{\mathrm{G}}[\tilde{\boldsymbol{r}}_{G_c/G}][\Phi_\rho][T]\ddot{\boldsymbol{\beta}} = &-m_{\mathrm{G}}[\tilde{\boldsymbol{r}}_{G_c/G}]\ddot{\boldsymbol{r}}_{P/N}\\ &- \left([I_{\mathrm{G},G}] - m_{\mathrm{G}}[\tilde{\boldsymbol{r}}_{G_c/G}]\left[\widetilde{[\Phi_\rho][T]\boldsymbol{\beta}}\right]\right)\dot{\boldsymbol{\omega}}_{\mathcal{P}/\mathcal{N}}\\ &+ \sum \boldsymbol{L}_G - \left[[\Phi_\theta][T]\dot{\boldsymbol{\beta}} + \boldsymbol{\omega}_{\mathcal{P}/\mathcal{N}}\right][I_{\mathrm{G},G}]\left([\Phi_\theta][T]\dot{\boldsymbol{\beta}} + \boldsymbol{\omega}_{\mathcal{P}/\mathcal{N}}\right)\\ &- [I_{\mathrm{G},G}][\tilde{\boldsymbol{\omega}}_{\mathcal{P}/\mathcal{N}}][\Phi_\theta][T]\dot{\boldsymbol{\beta}}\\ &- m_{\mathrm{G}}[\tilde{\boldsymbol{r}}_{G_c/G}]\left(2[\tilde{\boldsymbol{\omega}}_{\mathcal{P}/\mathcal{N}}][\Phi_\rho][T]\dot{\boldsymbol{\beta}} + [\tilde{\boldsymbol{\omega}}_{\mathcal{P}/\mathcal{N}}]^2[\Phi_\rho][T]\boldsymbol{\beta}\right)\end{aligned} \tag{46}$$

BACKSUBSTITUTION FORMULATION

Next, the general body equations of motion must be organized to facilitate integration with the hub equations of motion. Combining the general body equations yields

$$[\boldsymbol{M}_\beta]\ddot{\boldsymbol{\beta}} = [\boldsymbol{A}^{**}_\beta]\ddot{\boldsymbol{r}}_{P/N} + [\boldsymbol{B}^{**}_\beta]\dot{\boldsymbol{\omega}}_{\mathcal{P}/\mathcal{N}} + [\boldsymbol{C}^{**}_\beta] \tag{47}$$

where

$$[\boldsymbol{M}_\beta] = \begin{bmatrix} m_{\mathrm{G}}\left([\Phi_\rho] - \left[\tilde{\boldsymbol{r}}_{G_c/G}\right][\Phi_\theta]\right)[T] \\ \left([I_{\mathrm{G},G}][\Phi_\theta] + m_{\mathrm{G}}[\tilde{\boldsymbol{r}}_{G_c/G}][\Phi_\rho]\right)[T] \end{bmatrix} \tag{48}$$

$$[\boldsymbol{A}^{**}_\beta] = \begin{bmatrix} -m_{\mathrm{G}}[I_{3\times 3}] \\ -m_{\mathrm{G}}[\tilde{\boldsymbol{r}}_{G_c/G}] \end{bmatrix} \tag{49}$$

$$[\boldsymbol{B}^{**}_\beta] = \begin{bmatrix} m_{\mathrm{G}}\left[\boldsymbol{r}_{G_c/G}\widetilde{+[\Phi_\rho][T]\boldsymbol{\beta}}\right] \\ -\left([I_{\mathrm{G},G}] - m_{\mathrm{G}}[\tilde{\boldsymbol{r}}_{G_c/G}]\left[\widetilde{[\Phi_\rho][T]\boldsymbol{\beta}}\right]\right) \end{bmatrix} \tag{50}$$

$$[\boldsymbol{C}^{**}_\beta] = \begin{bmatrix} \sum \boldsymbol{F}_{\mathrm{G}} - 2m_{\mathrm{G}}[\tilde{\boldsymbol{\omega}}_{\mathcal{P}/\mathcal{N}}]\left([\Phi_\rho] - \left[\tilde{\boldsymbol{r}}_{G_c/G}\right][\Phi_\theta]\right)[T]\dot{\boldsymbol{\beta}} \\ -m_{\mathrm{G}}[\tilde{\boldsymbol{\omega}}_{\mathcal{P}/\mathcal{N}}]^2\left(\boldsymbol{r}_{G_c/G} + [\Phi_\rho][T]\boldsymbol{\beta}\right) - m_{\mathrm{G}}\left[\widetilde{[\Phi_\theta][T]\dot{\boldsymbol{\beta}}}\right]^2\boldsymbol{r}_{G_c/G} \\ \sum \boldsymbol{L}_G - \left[[\Phi_\theta][T]\dot{\boldsymbol{\beta}} + \boldsymbol{\omega}_{\mathcal{P}/\mathcal{N}}\right][I_{\mathrm{G},G}]\left([\Phi_\theta][T]\dot{\boldsymbol{\beta}} + \boldsymbol{\omega}_{\mathcal{P}/\mathcal{N}}\right) \\ -[I_{\mathrm{G},G}][\tilde{\boldsymbol{\omega}}_{\mathcal{P}/\mathcal{N}}][\Phi_\theta][T]\dot{\boldsymbol{\beta}} \\ -m_{\mathrm{G}}[\tilde{\boldsymbol{r}}_{G_c/G}]\left(2[\tilde{\boldsymbol{\omega}}_{\mathcal{P}/\mathcal{N}}][\Phi_\rho][T]\dot{\boldsymbol{\beta}} + [\tilde{\boldsymbol{\omega}}_{\mathcal{P}/\mathcal{N}}]^2[\Phi_\rho][T]\boldsymbol{\beta}\right) \end{bmatrix} \tag{51}$$

Next, Eq. 52 can be rewritten as

$$\ddot{\boldsymbol{\beta}} = [\boldsymbol{A}^{*}_\beta]\ddot{\boldsymbol{r}}_{P/N} + [\boldsymbol{B}^{*}_\beta]\dot{\boldsymbol{\omega}}_{\mathcal{P}/\mathcal{N}} + [\boldsymbol{C}^{*}_\beta] \tag{52}$$

where

$$[\boldsymbol{A}_\beta^*] = [\boldsymbol{M}_\beta]^{-1}[\boldsymbol{A}_\beta^{**}] \tag{53}$$
$$[\boldsymbol{B}_\beta^*] = [\boldsymbol{M}_\beta]^{-1}[\boldsymbol{B}_\beta^{**}] \tag{54}$$
$$[\boldsymbol{C}_\beta^*] = [\boldsymbol{M}_\beta]^{-1}[\boldsymbol{C}_\beta^{**}] \tag{55}$$

The prescribed body inertial accelerations are

$$\begin{aligned}\ddot{\boldsymbol{r}}_{P/N} &= \ddot{\boldsymbol{r}}_{P/B} + \ddot{\boldsymbol{r}}_{B/N} \\ &= \boldsymbol{r}''_{P/B} + 2[\tilde{\boldsymbol{\omega}}_{\mathcal{B}/\mathcal{N}}]\boldsymbol{r}'_{P/B} - [\tilde{\boldsymbol{r}}_{P/B}]\dot{\boldsymbol{\omega}}_{\mathcal{B}/\mathcal{N}} + [\tilde{\boldsymbol{\omega}}_{\mathcal{B}/\mathcal{N}}]^2\boldsymbol{r}_{P/B} + \ddot{\boldsymbol{r}}_{B/N} \qquad (56)\\ \dot{\boldsymbol{\omega}}_{\mathcal{P}/\mathcal{N}} &= \dot{\boldsymbol{\omega}}_{\mathcal{P}/\mathcal{B}} + \dot{\boldsymbol{\omega}}_{\mathcal{B}/\mathcal{N}} = \boldsymbol{\omega}'_{\mathcal{P}/\mathcal{B}} + [\tilde{\boldsymbol{\omega}}_{\mathcal{B}/\mathcal{N}}]\boldsymbol{\omega}_{\mathcal{P}/\mathcal{B}} + \dot{\boldsymbol{\omega}}_{\mathcal{B}/\mathcal{N}} \qquad (57)\end{aligned}$$

Substitution of Eqs. (56) and (57) into Eq. (52) gives the final form of the general body equations for backsubstitution into the hub equations of motion

$$\ddot{\boldsymbol{\beta}} = [\boldsymbol{A}_\beta]\ddot{\boldsymbol{r}}_{B/N} + [\boldsymbol{B}_\beta]\dot{\boldsymbol{\omega}}_{\mathcal{B}/\mathcal{N}} + [\boldsymbol{C}_\beta] \tag{58}$$

where

$$[\boldsymbol{A}_\beta] = [\boldsymbol{A}_\beta^*] \tag{59}$$
$$[\boldsymbol{B}_\beta] = [\boldsymbol{B}_\beta^*] - [\boldsymbol{A}_\beta^*][\tilde{\boldsymbol{r}}_{P/B}] \tag{60}$$
$$\begin{aligned}[\boldsymbol{C}_\beta] = [\boldsymbol{C}_\beta^*] &+ [\boldsymbol{A}_\beta^*]\left(\boldsymbol{r}''_{P/B} + 2[\tilde{\boldsymbol{\omega}}_{\mathcal{B}/\mathcal{N}}]\boldsymbol{r}'_{P/B} + [\tilde{\boldsymbol{\omega}}_{\mathcal{B}/\mathcal{N}}]^2\boldsymbol{r}_{P/B}\right) \\ &+ [\boldsymbol{B}_\beta^*]\left(\boldsymbol{\omega}'_{\mathcal{P}/\mathcal{B}} + [\tilde{\boldsymbol{\omega}}_{\mathcal{B}/\mathcal{N}}]\boldsymbol{\omega}_{\mathcal{P}/\mathcal{B}}\right)\end{aligned} \tag{61}$$

Back-substituting these results into the system equations of motion given by Eqs. (24) and (39) yields the final form of the system equations of motion

$$\begin{bmatrix}[A] & [B]\\ [C] & [D]\end{bmatrix}\begin{bmatrix}\ddot{\boldsymbol{r}}_{B/N}\\ \dot{\boldsymbol{\omega}}_{\mathcal{B}/\mathcal{N}}\end{bmatrix} = \begin{bmatrix}\boldsymbol{v}_{\text{trans}}\\ \boldsymbol{v}_{\text{rot}}\end{bmatrix} \tag{62}$$

The matrices are defined as

$$[A] = m_{\text{sc}}[I_{3\times3}] + m_{\text{G}}\left([\Phi_\rho] - \left[\tilde{\boldsymbol{r}}_{G_c/G}\right][\Phi_\theta]\right)[T][\boldsymbol{A}_\beta] \tag{63}$$
$$[B] = -m_{\text{sc}}[\tilde{\boldsymbol{c}}] + m_{\text{G}}\left([\Phi_\rho] - \left[\tilde{\boldsymbol{r}}_{G_c/G}\right][\Phi_\theta]\right)[T][\boldsymbol{B}_\beta] \tag{64}$$
$$\begin{aligned}[C] = m_{\text{sc}}[\tilde{\boldsymbol{c}}] &\\ + \Big([I_{\text{G},G_c}][\Phi_\theta] + m_{\text{G}}[\boldsymbol{r}_{G_c/G} &+ \widetilde{[\Phi_\rho][T]\boldsymbol{\beta} + \boldsymbol{r}_{P/B}}]\left([\Phi_\rho] - \left[\tilde{\boldsymbol{r}}_{G_c/G}\right][\Phi_\theta]\right)\Big)[T][\boldsymbol{A}_\beta]\end{aligned} \tag{65}$$
$$\begin{aligned}[D] = [I_{\text{sc},B}] &\\ + \Big([I_{\text{G},G_c}][\Phi_\theta] + m_{\text{G}}[\boldsymbol{r}_{G_c/G} &+ \widetilde{[\Phi_\rho][T]\boldsymbol{\beta} + \boldsymbol{r}_{P/B}}]\left([\Phi_\rho] - \left[\tilde{\boldsymbol{r}}_{G_c/G}\right][\Phi_\theta]\right)\Big)[T][\boldsymbol{B}_\beta]\end{aligned} \tag{66}$$

The vector components group the remaining terms

$$\boldsymbol{v}_{\text{trans}} = \sum \boldsymbol{F}_{\text{ext}} - 2m_{\text{sc}}[\tilde{\boldsymbol{\omega}}_{\mathcal{B}/\mathcal{N}}]\boldsymbol{c}' - m_{\text{sc}}[\tilde{\boldsymbol{\omega}}_{\mathcal{B}/\mathcal{N}}]^2\boldsymbol{c}$$

Prescribed contributions $\Big\{ -m_{\text{P}}\boldsymbol{r}''_{P_c/B}$

$$
\begin{aligned}
\text{General body contr.} & \left\{ -m_{\mathrm{G}} \left[\widetilde{[\Phi_\theta][T]\dot{\boldsymbol{\beta}}} \right]^2 \boldsymbol{r}_{G_c/G} - m_{\mathrm{G}} \left([\Phi_\rho] - \left[\tilde{\boldsymbol{r}}_{G_c/G} \right] [\Phi_\theta] \right) [T][\boldsymbol{C}_\beta] \right. \\
\text{Coupling contr.} & \left\{ \begin{array}{l} - m_{\mathrm{G}} \left(2[\tilde{\boldsymbol{\omega}}_{\mathcal{P}/\mathcal{B}}] \left([\Phi_\rho] - \left[\tilde{\boldsymbol{r}}_{G_c/G} \right] [\Phi_\theta] \right) [T]\dot{\boldsymbol{\beta}} \right. \\ \left. + \left([\tilde{\boldsymbol{\omega}}'_{\mathcal{P}/\mathcal{B}}] + [\tilde{\boldsymbol{\omega}}_{\mathcal{P}/\mathcal{B}}]^2 \right) \left(\boldsymbol{r}_{G_c/G} + [\Phi_\rho][T]\boldsymbol{\beta} \right) + \boldsymbol{r}''_{P/B} \right) \end{array} \right.
\end{aligned}
\tag{67}
$$

$$
\begin{aligned}
\boldsymbol{v}_{\text{rot}} &= \sum \boldsymbol{L}_B - \left([I'_{\text{sc},B}] + [\tilde{\boldsymbol{\omega}}_{\mathcal{B}/\mathcal{N}}][I_{\text{sc},B}] \right) \boldsymbol{\omega}_{\mathcal{B}/\mathcal{N}} \\
\text{Prescribed contributions} & \left\{ \begin{array}{l} - [I_{\mathrm{P},P_c}]\boldsymbol{\omega}'_{\mathcal{P}/\mathcal{B}} - m_{\mathrm{P}}[\tilde{\boldsymbol{r}}_{P_c/B}]\boldsymbol{r}''_{P_c/B} \\ - [\tilde{\boldsymbol{\omega}}_{\mathcal{P}/\mathcal{N}}][I_{\mathrm{P},P_c}]\boldsymbol{\omega}_{\mathcal{P}/\mathcal{B}} - m_{\mathrm{P}}[\tilde{\boldsymbol{\omega}}_{\mathcal{B}/\mathcal{N}}][\tilde{\boldsymbol{r}}_{P_c/B}]\boldsymbol{r}'_{P_c/B} \end{array} \right. \\
\text{General body contr.} & \left\{ \begin{array}{l} - m_{\mathrm{G}}[\boldsymbol{r}_{G_c/G} \widetilde{+ [\Phi_\rho]}[T]\boldsymbol{\beta}] \left[\widetilde{[\Phi_\theta][T]\dot{\boldsymbol{\beta}}} \right]^2 \boldsymbol{r}_{G_c/G} \\ - \left[[\Phi_\theta]\widetilde{[T]\dot{\boldsymbol{\beta}} + \boldsymbol{\omega}_{\mathcal{P}/\mathcal{N}}} \right] [I_{\mathrm{G},G_c}][\Phi_\theta][T]\dot{\boldsymbol{\beta}} \\ - m_{\mathrm{G}}[\tilde{\boldsymbol{\omega}}_{\mathcal{P}/\mathcal{N}}] \left[\boldsymbol{r}_{G_c/G} \widetilde{+ [\Phi_\rho]}[T]\boldsymbol{\beta} \right] \left([\Phi_\rho] - \left[\tilde{\boldsymbol{r}}_{G_c/G} \right] [\Phi_\theta] \right) [T]\dot{\boldsymbol{\beta}} \\ - \left([I_{\mathrm{G},G_c}][\Phi_\theta] + m_{\mathrm{G}}[\boldsymbol{r}_{G_c/G} + \widetilde{[\Phi_\rho]}[T]\boldsymbol{\beta} + \boldsymbol{r}_{P/B}] \left([\Phi_\rho] - \left[\tilde{\boldsymbol{r}}_{G_c/G} \right] [\Phi_\theta] \right) \right) [T][\boldsymbol{C}_\beta] \end{array} \right. \\
\text{Coupling contr.} & \left\{ \begin{array}{l} - [I_{\mathrm{G},G_c}] \left([\tilde{\boldsymbol{\omega}}_{\mathcal{P}/\mathcal{B}}][\Phi_\theta][T]\dot{\boldsymbol{\beta}} + \boldsymbol{\omega}'_{\mathcal{P}/\mathcal{B}} \right) - \left[[\Phi_\theta]\widetilde{[T]\dot{\boldsymbol{\beta}} + \boldsymbol{\omega}_{\mathcal{P}/\mathcal{N}}} \right] [I_{\mathrm{G},G_c}]\boldsymbol{\omega}_{\mathcal{P}/\mathcal{B}} \\ - m_{\mathrm{G}}[\tilde{\boldsymbol{r}}_{P/B}] \left[\widetilde{[\Phi_\theta][T]\dot{\boldsymbol{\beta}}} \right]^2 \boldsymbol{r}_{G_c/G} \\ - m_{\mathrm{G}} \left[\boldsymbol{r}_{G_c/G} + \widetilde{[\Phi_\rho][T]}\boldsymbol{\beta} + \boldsymbol{r}_{P/B} \right] \left(2[\tilde{\boldsymbol{\omega}}_{\mathcal{P}/\mathcal{B}}] \left([\Phi_\rho] - \left[\tilde{\boldsymbol{r}}_{G_c/G} \right] [\Phi_\theta] \right) [T]\dot{\boldsymbol{\beta}} \right. \\ \left. + \left([\tilde{\boldsymbol{\omega}}'_{\mathcal{P}/\mathcal{B}}] + [\tilde{\boldsymbol{\omega}}_{\mathcal{P}/\mathcal{B}}]^2 \right) \left(\boldsymbol{r}_{G_c/G} + [\Phi_\rho][T]\boldsymbol{\beta} \right) + \boldsymbol{r}''_{P/B} \right) \\ - m_{\mathrm{G}} \left([\tilde{\boldsymbol{\omega}}_{\mathcal{B}/\mathcal{N}}][\tilde{\boldsymbol{r}}_{P/B}] - [\tilde{\boldsymbol{\omega}}_{\mathcal{P}/\mathcal{B}}] \left[\boldsymbol{r}_{G_c/G} \widetilde{+ [\Phi_\rho]}[T]\boldsymbol{\beta} \right] \right) \left([\Phi_\rho] - \left[\tilde{\boldsymbol{r}}_{G_c/G} \right] [\Phi_\theta] \right) [T]\dot{\boldsymbol{\beta}} \\ - m_{\mathrm{G}}[\tilde{\boldsymbol{\omega}}_{\mathcal{B}/\mathcal{N}}] \left[\boldsymbol{r}_{G_c/G} + \widetilde{[\Phi_\rho][T]}\boldsymbol{\beta} + \boldsymbol{r}_{P/B} \right] \left([\tilde{\boldsymbol{\omega}}_{\mathcal{P}/\mathcal{B}}] \left(\boldsymbol{r}_{G_c/G} + [\Phi_\rho][T]\boldsymbol{\beta} \right) + \boldsymbol{r}'_{P/B} \right) \end{array} \right.
\end{aligned}
\tag{68}
$$

The backsubstitution contributions above can be implemented and numerically integrated in software to simulate any type of joint motion relative to a prescribed component.

NUMERICAL SIMULATION

This section provides a spacecraft simulation scenario demonstrating the applicability of the branching dynamics derived in the previous section. Recall that any type of 6-DOF rigid body joint motion can be simulated using these results. A revolute (1-DOF rotational) joint is chosen for the numerical simulation presented in this paper. Substitution of the revolute joint information provided in Table 1 into the general branching equations of motion provides the specific backsubstitution dynamics for the single-axis spinning body chained system derived and verified in prior work.[52] The backsubstitution dynamics for the single-axis spinning body chained system are implemented in the Basilisk [‡] astrodynamics simulation software. Note that the existing

[‡] `https://avslab.github.io/basilisk`

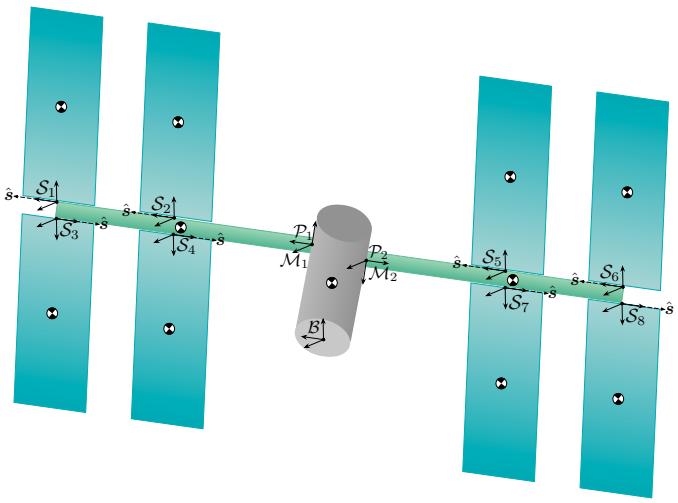

Figure 3. Spacecraft system simulation configuration.

Table 2. Hub simulation parameters.

Parameter	Notation	Value	Unit
Hub mass	m_{hub}	15,000	kg
Hub inertia about its center of mas	${}^{\mathcal{B}}[I_{\text{hub},B_c}]$	$\begin{bmatrix} 580,000 & 0 & 0 \\ 0 & 160,000 & 0 \\ 0 & 0 & 580,000 \end{bmatrix}$	kg $\cdot$ m^2
Hub center of mass location with respect to point B	${}^{\mathcal{B}}\boldsymbol{r}_{B_c/B}$	[0, 0, 0]	m
Hub initial inertial angular velocity	${}^{\mathcal{B}}\boldsymbol{\omega}_{\mathcal{B}/\mathcal{N}}$	[0, 0, 0]	rad / s

`spinningBodyOneDOFStateEffector` software had to be expanded to include the coupling terms shown in Eqs. (67) and (68). Additionally, the `stateEffector` base class was cleanly modified to allow connection of the spinning body and other effectors to the prescribed component. The full simulation is openly available online as a Basilisk example scenario [§].

The spacecraft configuration selected for the simulation is illustrated in Fig. (3). The simulation sets up an ISS-scale spacecraft containing a cylindrical rigid hub (gray), two large prescribed trusses (green) which rotate about their longitudinal axes, and eight single-axis solar panels (blue) which rotate about their transverse (bending) axes. The truss body ($\mathcal{P}$) and mount ($\mathcal{M}$) frames are initially aligned, as seen in Fig. (3). The hub, truss, and solar panel structures each have dimensions 8x8x20 , 50x4x4, and 10x0.3x30 meters, respectively. Other relevant parameters for the hub, trusses, and solar panels are provided in Tables 2-4.

The spacecraft is at rest at the start of the simulation with the configuration seen in Fig. (3). To demonstrate the impact of the prescribed truss motion on the solar panel dynamics, all solar panels are given zero initial deflections. The trusses are profiled to symmetrically rotate 45 degrees from

[§]Data available online at https://avslab.github.io/basilisk/examples/scenarioPrescribedMotionWithRotationBranching.html

Table 3. Prescribed truss parameters.

Parameter	Notation	Value	Unit
Truss mass	m_{P}	6000	kg
Truss inertia about its center of mass	${}^{\mathcal{P}}[I_{\mathrm{P},P_c}]$	$\begin{bmatrix} 1,258,000 & 0 & 0 \\ 0 & 1,258,000 & 0 \\ 0 & 0 & 16,000 \end{bmatrix}$	kg · m^2
Truss center of mass locations with respect to points P	${}^{\mathcal{P}}\boldsymbol{r}_{P_c/P}$	[25, 0, 0]	m
Truss 1 mount frame location with respect to point B	${}^{\mathcal{B}}\boldsymbol{r}_{M_1/B}$	[4, 0, 0]	m
Truss 2 mount frame location with respect to point B	${}^{\mathcal{B}}\boldsymbol{r}_{M_2/B}$	[-4, 0, 0]	m
DCM of mount frame 1 with respect to the $\mathcal{B}$ frame	$[\mathcal{M}_1\mathcal{B}]$	$\begin{bmatrix} 1 & 0 & 0 \\ 0 & 1 & 0 \\ 0 & 0 & 1 \end{bmatrix}$	—
DCM of mount frame 2 with respect to the $\mathcal{B}$ frame	$[\mathcal{M}_2\mathcal{B}]$	$\begin{bmatrix} -1 & 0 & 0 \\ 0 & 1 & 0 \\ 0 & 0 & -1 \end{bmatrix}$	—
Truss rotation axes	${}^{\mathcal{M}}\hat{\boldsymbol{p}}_\theta$	[1, 0, 0]	—

Table 4. Solar panel parameters.

Parameter	Notation	Value	Unit
Panel mass	m_{S}	1000	kg
Panel inertia about its center of mass	${}^{\mathcal{S}}[I_{\mathrm{S},S_c}]$	$\begin{bmatrix} 83,333.333 & 0 & 0 \\ 0 & 8,340.833 & 0 \\ 0 & 0 & 76,333.333 \end{bmatrix}$	kg · m^2
Panel center of mass locations with respect to points S	${}^{\mathcal{S}}\boldsymbol{r}_{S_c/S}$	[0, 0, 15]	m
Panel bending rotation axes	${}^{\mathcal{S}}\hat{\boldsymbol{s}}$	[1, 0, 0]	—
Torsional spring constant	k	$7 \cdot 10^5$	N · m / rad
Torsional damper constant	c	$5 \cdot 10^4$	N · m · s / rad

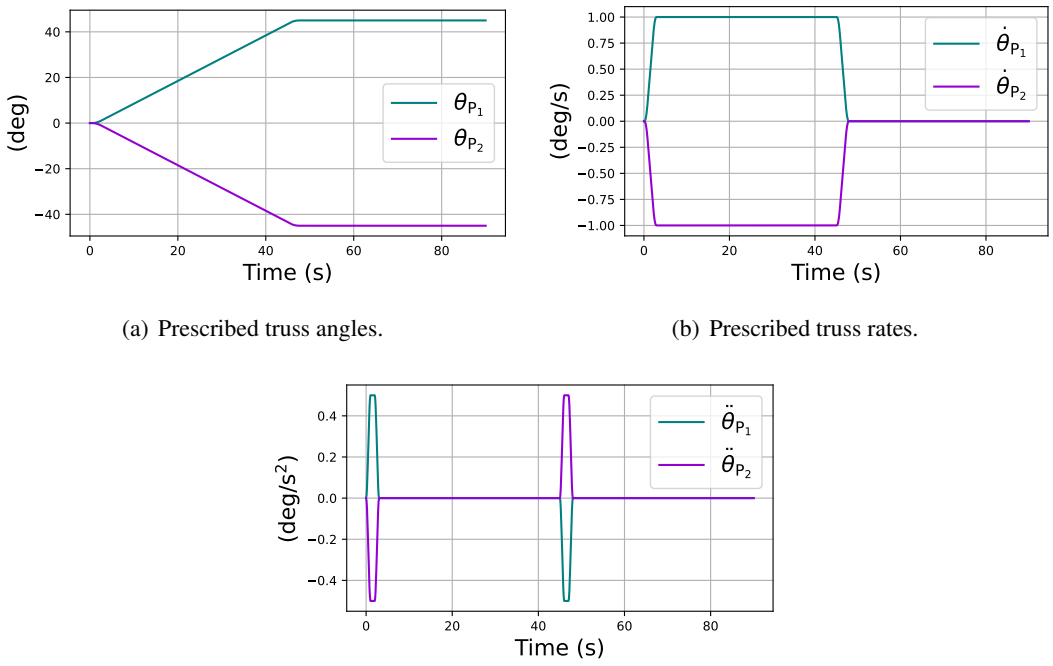

(a) Prescribed truss angles.

(b) Prescribed truss rates.

(c) Prescribed truss accelerations.

Figure 4. Prescribed truss motion.

their initial configurations using a smoothed bang-coast-bang acceleration profile.[51] The prescribed truss motion is provided in Fig. (4), where the truss angles are seen in Fig. 4(a), their rates are seen in Fig. 4(b), and their accelerations are seen in Fig. 4(c).

The impact of the prescribed truss motion on the solar panel dynamics is provided in Fig. (5). The solar panel angles are given in Fig. 5(a) and their rates are seen in Fig. 5(b). The panels mounted to the top of the truss structure (panels 1, 2, 5 and 6) are observed to deflect negatively relative to their spin axes, while the panels mounted to the bottom of the trusses (panels 3, 4, 7 and 8) deflect positively about their spin axes. The observed panel motion is expected, indicating that the truss rotation directly impacts the bending angle of the panels.

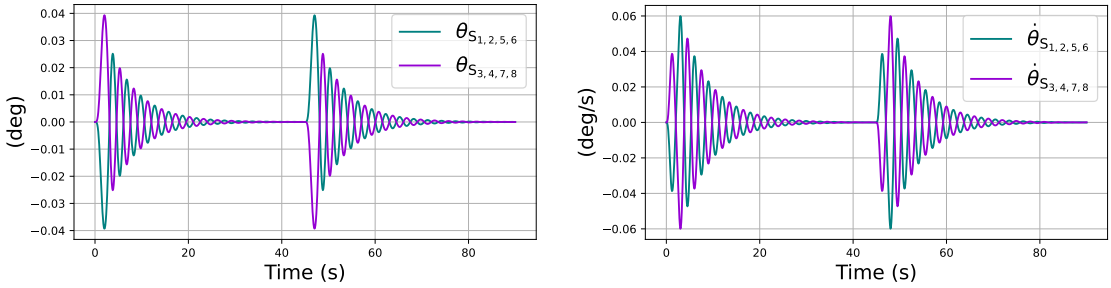

(a) Panel bending angles.

(b) Panel bending rates.

Figure 5. Solar panel response.

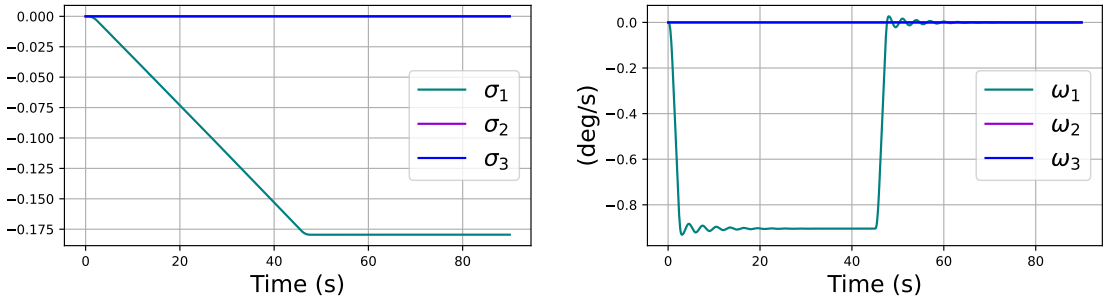

(a) Hub inertial attitude $\boldsymbol{\sigma}_{\mathcal{B}/\mathcal{N}}$.

(b) Hub inertial angular velocity ${}^{\mathcal{B}}\boldsymbol{\omega}_{B/N}$.

Figure 6. Hub response.

Finally, the hub response to the truss and panel motion is illustrated in Fig. (6). Its inertial attitude and angular velocity are provided in Figs. 6(a) and 6(b). Because the spacecraft is simulated in a conservative environment, its motion is expected to respond in order to conserve the angular momentum about its center of mass. Viewing Figs. 6(a) and 6(b), the hub is seen to rotate about its first (longitudinal axis) negatively throughout the simulation, which indeed opposes the prescribed truss motion. The hub angular velocity is seen to oscillate during the acceleration periods of the truss motion and returns to zero after the truss actuation is complete, confirming the expected response.

CONCLUSION

Building on prior work which developed branching formulations for attachment of specific constrained spacecraft components to prescribed motion components using the backsubstitution method, this work develops a generalized backsubstitution formulation for attaching general free rigid bodies to prescribed components using a joint mapping representation. The results can be implemented in software to simulate any type of six degree-of-freedom joint motion relative to a prescribed component. Future work involves implementing the general equations into software and verifying the results using energy and momentum verifications.

REFERENCES

[1] C. R. Mercer, "Chapter Twelve - Solar array designs for deep space science missions," *Photovoltaics for Space* (S. G. Bailey, A. F. Hepp, D. C. Ferguson, R. P. Raffaelle, and S. M. Durbin, eds.), pp. 349–378, Elsevier, 2023, 10.1016/B978-0-12-823300-9.00006-6.

[2] J. Gibb, "Lightweight Flexible Space Solar Arrays, Past, Present and Future," *2018 IEEE 7th World Conference on Photovoltaic Energy Conversion (WCPEC) (A Joint Conference of 45th IEEE PVSC, 28th PVSEC & 34th EU PVSEC)*, 2018, pp. 3530–3534, 10.1109/PVSC.2018.8547918.

[3] J. Sun, "A New Design of the 3D Deployable Solar Array in the Aerospace Field and Kinematic Analysis during Deployment," *Journal of Physics: Conference Series*, Vol. 2364, nov 2022, p. 012039, 10.1088/1742-6596/2364/1/012039.

[4] J. Parker, F. Hameli, J. Knittel, M. Caudill, S. Chikine, S. Baskar, A. Koehler, and P. Imler, "The Preliminary Mission Design of the Emirates Mission to Explore the Asteroids (EMA)," *AAS Guidance and Control Conference*, Feb. 2–7 2024. Paper No. AAS 24-064.

[5] R. Calaon, C. Allard, and H. Schaub, "Solar Electric Propulsion GN&C Pointing State Overview For The Emirates Mission To The Asteroid Belt," *AAS Guidance and Control Conference*, Breckenridge, CO, Feb. 2–7 2024. Paper No. AAS 24-056.

[6] A. Cheng, J. Atchison, B. Kantsiper, A. Rivkin, A. Stickle, C. Reed, A. Galvez, I. Carnelli, P. Michel, and S. Ulamec, "Asteroid Impact and Deflection Assessment mission," *Acta Astronautica*, Vol. 115, 2015, pp. 262–269.

[7] M. K. Chamberlain, S. H. Kiefer, M. LaPointe, and P. LaCorte, "On-orbit flight testing of the Roll-Out Solar Array," *Acta Astronautica*, Vol. 179, 2021, pp. 407–414.

[8] J. R. Brophy, "NASA's Deep Space 1 Ion Engine (Plenary)," *Review of Scientific Instruments*, Vol. 73, No. 2, 2002, pp. 1071–1078.

[9] B. N. M. M. M. H. J. Brophy, C. Garner and D. Noon, "General Hinged Rigid-Body Dynamics Approximating First-Order Spacecraft Solar Panel Flexing," *The Ion Propulsion System for Dawn*, Vol. 55, 2003, p. 4542.

[10] T. D. W. H. T. I. e. a. D. Y. Oh, S. Collins, "Development of the Psyche Mission for NASA's Discovery Program," *36th International Electric Propulsion Conference*, University of Vienna, Vienna Austria, Sep. 15–20 2019. Paper No. IEPC-2019-192.

[11] J. S. Sovey, V. K. Rawlin, and M. J. Patterson, "Ion Propulsion Development Projects in U.S.: Space Electric Rocket Test I to Deep Space 1," *Journal of Propulsion and Power*, Vol. 17, No. 3, 2001, pp. 517–526, 10.2514/2.5806.

[12] R. Calaon, L. Kiner, C. Allard, and H. Schaub, "Momentum Management Of A Spacecraft Equipped With A Dual-Gimballed Electric Thruster," *AAS Guidance and Control Conference*, Breckenridge, CO, Feb. 2–8 2023. Paper No. AAS-23-178.

[13] L. Kiner, C. Allard, and H. Schaub, "Two-Axis Gimbal Simulation Overview For The Emirates Mission To The Asteroid Belt," *AAS Guidance, Navigation and Control Conference*, Breckenridge, CO, Jan. 31 – Feb. 5 2025. Paper No. AAS-25-013.

[14] NASA, "Canadarm2," `https://images.nasa.gov/details/iss073e0546366`, 2025. [Accessed 23-Dec-2025].

[15] NASA, "EMA MBR Explorer," `https://space.gov.ae/en/projects-and-initiatives/space-exploration/emirates-mission-to-the-asteroid-belt`, 2025. [Accessed 23-Dec-2025].

[16] R. G. D. B. A. Aikenhead and F. M. Davis, "Canadarm and The Space Shuttle," *Journal of Vacuum Science and Technology A: Vacuum, Surfaces, and Films*, Vol. 1, No. 2, 1983, pp. 126–132.

[17] S. Sachdev, "Canadarm- a review of its flights," *Journal of Vacuum Science and Technology A: Vacuum, Surfaces, and Films*, Vol. 4, No. 3, 1986, pp. 268–272.

[18] A. K. Banerjee, "Contributions of Multibody Dynamics to Space Flight: A Brief Review," *Journal of Guidance, Control, and Dynamics*, Vol. 26, No. 3, 2003, pp. 385–394, 10.2514/2.5069.

[19] W. W. Hooker, "A Set of r Dynamical Attitude Equations for an Arbitrary n-Body Satellite Having r Rotational Degrees of Freedom," *AIAA Journal*, Vol. 8, No. 7, 1970, pp. 1205–1207, 10.2514/3.5873.

[20] V. J. Modi, "Attitude Dynamics of Satellites with Flexible Appendages—A Brief Review," *Journal of Spacecraft and Rockets*, Vol. 11, No. 11, 1974, pp. 743–751, 10.2514/3.62172.

[21] P. W. Likins, "Point-connected Rigid Bodies in a Topological Tree," *Celestial Mechanics*, Vol. 11, No. 3, 1975, pp. 301–317, 10.1007/BF01228809.

[22] B. Paul, "Analytical dynamics of mechanisms—a computer oriented overview," *Mechanism and Machine Theory*, Vol. 10, No. 6, 1975, pp. 481–507, 10.1016/0094-114X(75)90005-1.

[23] W. Jerkovsky, "The Structure of Multibody Dynamics Equations," *Journal of Guidance and Control*, Vol. 1, No. 3, 1978, pp. 173–182, 10.2514/3.55761.

[24] J. Y. S. Luh, M. W. Walker, and R. P. C. Paul, "On-Line Computational Scheme for Mechanical Manipulators," *Journal of Dynamic Systems, Measurement, and Control*, Vol. 102, June 1980, pp. 69–76, 10.1115/1.3149599.

[25] M. W. Walker and D. E. Orin, "Efficient Dynamic Computer Simulation of Robotic Mechanisms," *Journal of Dynamic Systems, Measurement, and Control*, Vol. 104, Sept. 1982, pp. 205–211, 10.1115/1.3139699.

[26] A. Jain, "Unified Formulation of Dynamics for Serial Rigid Multibody System," *Journal of Guidance, Control, and Dynamics*, Vol. 14, No. 3, 1991, pp. 531–542, 10.2514/3.20672.

[27] K. Anderson, "An Order N Formulation for the Motion Simulation of General Multi-Rigid-Body Tree Systems," *Computers & Structures*, Vol. 46, No. 3, 1993, pp. 547–559, 10.1016/0045-7949(93)90224-2.

[28] S. Pradhan, V. J. Modi, and A. K. Misra, "Order N Formulation for Flexible Multibody Systems in Tree Topology: Lagrangian Approach," *Journal of Guidance, Control, and Dynamics*, Vol. 20, No. 4, 1997, pp. 665–672, 10.2514/2.4129.

[29] J. Critchley and K. S. Anderson, "A Generalized Recursive Coordinate Reduction Method for Multibody System Dynamics," *International Journal for Multiscale Computational Engineering*, Vol. 1, No. 2&3, 2003, 10.1615/IntJMultCompEng.v1.i23.50.

[30] M. J. Sidi, *Spacecraft Dynamics and Control: A Practical Engineering Approach*, Vol. 7. Cambridge University Press, 1997.

[31] H. Schaub and J. L. Junkins, *Analytical Mechanics of Space Systems*. Reston, Virginia: American Institute of Aeronautics and Astronautics, Inc., 4 ed., 2018.

[32] R. Featherstone, *Rigid Body Dynamics Algorithms*. Springer New York, 2008, 10.1007/978-1-4899-7560-7.

[33] R. Featherstone, "The Calculation of Robot Dynamics Using Articulated-Body Inertias," *The International Journal of Robotics Research*, Vol. 2, No. 1, 1983, pp. 13–30, 10.1177/027836498300200102.

[34] R. Featherstone, *Robot Dynamics Algorithms*. Springer New York, NY, 1987, 10.1007/978-0-387-74315-8.

[35] M. Brady, J. M. Hollerbach, T. L. Johnson, T. Lozano-Pérez, and M. T. Mason, eds., *Robot Motion: Planning and Control*. Cambridge, MA: The MIT Press, 1982.

[36] G. Rodriguez, A. Jain, and K. Kreutz-Delgado, "A Spatial Operator Algebra for Manipulator Modeling and Control," *The International Journal of Robotics Research*, Vol. 10, No. 4, 1991, pp. 371–381, 10.1177/027836499101000406.

[37] A. Jain and G. Rodriguez, "Recursive Flexible Multibody Dynamics Using Spatial Operators," Vol. 16, 1993, pp. 345–358, 10.1016/B978-0-444-89856-2.50036-3.

[38] A. Jain, *Robot and Multibody Dynamics: Analysis and Algorithms*. Springer Science & Business Media, 2010.

[39] C. Allard, M. D. Ramos, H. Schaub, P. Kenneally, and S. Piggott, "Modular Software Architecture for Fully Coupled Spacecraft Simulations," *Journal of Aerospace Information Systems*, Vol. 15, No. 12, 2018, pp. 670–683.

[40] P. W. Kenneally, S. Piggott, and H. Schaub, "Basilisk: A Flexible, Scalable and Modular Astrodynamics Simulation Framework," *Journal of Aerospace Information Systems*, Vol. 17, Sept. 2020, pp. 496–507.

[41] C. Allard, M. D. Ramos, and H. Schaub, "Computational Performance of Complex Spacecraft Simulations Using Back-Substitution," *Journal of Aerospace Information Systems*, Vol. 16, No. 10, 2019, pp. 427–436.

[42] J. Vaz Carneiro and H. Schaub, "Spacecraft Dynamics With The Backsubstitution Method: Survey And Capabilities," *AAS Spaceflight Mechanics Meeting*, Kauai, Hawaii, Jan. 19–23 2025. Paper No. AAS 25-232.

[43] C. Allard, H. Schaub, and S. Piggott, "General Hinged Rigid-Body Dynamics Approximating First-Order Spacecraft Solar Panel Flexing," *Journal of Spacecraft and Rockets*, Vol. 55, No. 5, 2018, pp. 1290–1298.

[44] J. Alcorn, C. Allard, and H. Schaub, "Fully Coupled Reaction Wheel Static and Dynamic Imbalance for Spacecraft Jitter Modeling," *AIAA Journal of Guidance, Control, and Dynamics*, Vol. 41, No. 6, 2018, pp. 1380–1388, 10.2514/1.G003277.

[45] J. Alcorn, C. Allard, and H. Schaub, "Fully-Coupled Dynamical Jitter Modeling Of Variable-Speed Control Moment Gyroscopes," *AAS/AIAA Astrodynamics Specialist Conference*, Stevenson, WA, Aug. 20–24 2017. Paper No. AAS-17-730.

[46] C. Allard, M. Diaz-Ramos, and H. Schaub, "Spacecraft Dynamics Integrating Hinged Solar Panels and Lumped-Mass Fuel Slosh Model," *AIAA/AAS Astrodynamics Specialist Conference*, Long Beach, CA, Sept. 12–15 2016.

[47] P. Cappuccio, C. Allard, and H. Schaub, "Fully-Coupled Spherical Modular Pendulum Model To Simulate Spacecraft Propellant Slosh," *AAS/AIAA Astrodynamics Specialist Conference*, Snowbird, UT, August 19–23 2018. Paper No. AAS-18-224.

[48] J. Vaz Carneiro, C. Allard, and H. Schaub, "General Dynamics for Single- and Dual-Axis Rotating Rigid Spacecraft Components," *Journal of Spacecraft and Rockets*, Vol. 61, July–August 2024, pp. 1099–1113, 10.2514/1.A35865.

[49] J. Vaz Carneiro, C. Allard, and H. Schaub, "Effector Dynamics For Sequentially Rotating Rigid Body Spacecraft Components," *AAS/AIAA Astrodynamics Specialist Conference*, Big Sky, MO, Aug. 13–17 2023. Paper AAS 23–192.

[50] J. Vaz Carneiro, P. Johnson, and H. Schaub, "Backsubstitution Method For Spacecraft With Generally Translating Appendages," *AAS Astrodynamics Specialist Conference*, Broomfield, CO, Aug. 11–15 2024. Paper No. AAS 24-248.

[51] L. Kiner, H. Schaub, and C. Allard, "Spacecraft Backsubstitution Dynamics with General Multibody Prescribed Subcomponents," *Journal of Aerospace Information Systems*, Vol. 22, August 2025, pp. 703–715, 10.2514/1.I011491.

[52] L. Kiner and H. Schaub, "Backsubstitution Method For Prescribed Motion Actuators With Attached Dynamic Sub-Components," *AAS/AIAA Astrodynamics Specialist Conference*, Boston, MA, August 10–14 2025. Paper No. AAS 25-790.